Master Thesis in Geographical Information Science nr 106

Analysis of spatial-temporal pattern of Land Surface Temperature (LST) due to NDVI and elevation in Ilorin, Nigeria

Elijah Akwarandu NJOKU

2019

Department of

Physical Geography and Ecosystem Science

Centre for Geographical Information Systems

Lund University

Njoku, E.A (2019) **Analysis of spatial-temporal pattern of Land Surface Temperature (LST) due to NDVI and elevation in Ilorin, Nigeria**
Master's degree thesis, 30/ credits in Geographical Information Science (GIS)
Department of Physical Geography and Ecosystem Science, Lund University

Analysis of spatial-temporal pattern of Land Surface Temperature (LST) due to NDVI and elevation in Ilorin, Nigeria

Elijah Akwarandu NJOKU

Master's degree thesis, 30 credits in Master in Geographical Information Science, Centre for Geographical Information System, Department of Physical Geography and Ecosystem Science, Lund University, Sweden.

Supervisor

Dr. David E. Tenenbaum
Department of Physical Geography and Ecosystem Science,
Lund University.

Examination Committee

Dr. Ulrik Mårtensson
Department of Physical Geography and Ecosystem Science
Lund University

and
Dr. Anna Maria Jönsson
Department of Physical Geography and Ecosystem Science
Lund University

Abstract

The rate of global urbanization in the 21st century has been unprecedented especially in the African and the Asian continents. Urbanization typically causes a removal of natural vegetation and replacement of same with impervious and non-evaporative urban materials with high heat capacity and low solar reflectivity. The alteration of the natural land cover due to urbanization causes a change in the thermal properties of the urban landscape, with the effect that the urban land surface typically has a relatively higher thermal capacity than that of the surrounding rural areas; a phenomenon known as Urban Heat Island (UHI).

Studies have shown that, in the last few decades, Ilorin city has undergone significant changes in landscape, population structure, and urban form and the city has witnessed a rise in urban temperature. Similarly, Nigerian Meteorological Agency (NIMET) and epidemiologists have warned of possible outbreak of some diseases that thrive in hot weather such as meningitis, tuberculosis, malaria, dengue fever, etc. Given this scenario, UHI effects is estimated to affect a large number of persons in the city. This study investigates to what extent the observed Land Surface Temperature (LST) could be accounted for by vegetation cover measured via Normalized Difference Vegetation Index (NDVI) in the study area from 2000 to 2016. The spatial pattern and trend of LST, and the magnitude of UHI within the period was also estimated.

Result shows a statistically significant clustering of LST values in all the investigated epochs with Global Moran's I index showing values greater than 0.6 and z-scores greater than 220 in all cases at $p < 0.001$. Analysis of regression reveals that NDVI explained between 50% - 71% of the variation in LST between 2000 and 2002, and NDVI increasingly diminished in importance as an explanatory variable for LST in 2016, where only 29% - 49% explanation was provided by NDVI. For all the seasons and years, the coefficients of the regression analysis results for NDVI in the study area are negative indicating that NDVI is inversely related to LST. Research result shows a presence of UHI with an intensity ranging between 0.2^{o}C to 4.6^{o}C, with peaks in the wet seasons and tending towards a decreasing trend.

Keywords: GIS, Land Surface Temperature, NDVI, Ilorin, Elevation, Urban Heat Island

Acknowledgement

I am sincerely grateful to my supervisor, Dr David Tenenbaum who also doubled as the programme coordinator, for his immense support in this thesis and the programme in general. I especially appreciate his penchant for quality work and his very short turnaround time in evaluating my submissions. Very many thanks to my colleagues, especially Boris and Senait for making themselves available for incisive technical discussions throughout the program duration.

Special thanks to my dear wife who provided immense support at different fronts as the programme lasted. I am infinitely grateful to Jehovah God for keeping me alive and seeing me through my journey in Sweden.

Table of Contents

List of Abbreviation

UN	United Nations
LST	Land Surface Temperature
UHI	Urban Heat Island
LCLU	Land cover land use
NiMet	Nigeria Meteorological Agency
NDVI	Normalized Difference Vegetation Index
CLHI	Canopy Layer Heat Island
BLHI	Boundary Layer Heat Island
SUHI	Surface Urban Heat Island
NDBal	Normalized Difference Barrenness Index
NDWI	Normalized Difference Water Index
NDBI	Normalized Difference Built-up Index
TM	Thematic Mapper
ETM+	Enhanced Thematic Mapper Plus
OLI	Operational Land Imager
MODIS	Moderate Resolution Imaging Spectro-radiometer
AVHRR	Advanced Very High Resolution Radiometer
ASTER	Advanced Space-borne Thermal Emission and Reflection
GEOS	Geostationary Operational Environmental Satellites
SPOT	Satellite Pour l'Observation la Terre
USGS	United States Geological Survey
DEM	Digital Elevation Model
ASF	Alaska Satellite Facility

SRTM	Shuttle radar Topography Mission
NED1	National Elevation Dataset-1
NED2	National Elevation Dataset-2
NGS	National Geodetic Survey
RTC	Radiometrically and Terrain Corrected
ESRI	Environmental Systems Research Institute
RGB	Red Green Blue
DOS-1	Dark Object Subtraction-1
QGIS	Quantum GIS
MLCA	Maximum Likelihood Classification Algorithm
TOA	Top of Atmosphere
NPC	National Population Commission
OLS	Ordinary Least Squares

List of Figures

List of Tables

List of Plates

CHAPTER ONE

1.0 Background

The 21st century has witnessed an unprecedented rate of urbanization and global urban population growth, especially in the African and the Asian continents. At present, it is estimated that more than 50 percent of the global population lives in cities, and that number is projected to reach 66 percent in 2050 (UN, 2016). People are attracted to urban areas for several reasons. While the increased economic activities in the urban areas have been a pull factor for some, others have preferred living in the cities because of the abundant life-support infrastructure and bustling social life in the cities.

Despite its advantages, however, urbanization is associated with various socioeconomic and environmental challenges. When coupled with the impacts of climate change the twin phenomena of urbanization and population growth can put significant pressure on cities' physical and social environments. One of the most common consequences of urbanization is the formation of an Urban Heat Island (UHI) (García-Díez et al., 2016).

The UHI is the relative elevation of urban ambient air and surface temperature over its rural surrounding (Oke, 1982; Voogt and Oke, 2003). At a detailed scale of analysis, a complex mix of variables and factors are known to cause and affect the urban heat island phenomenon (Oke, 1982; Zhao et al. 2014). However, several studies have shown that Land Cover/Land Use (LCLU) is directly linked with Land Surface Temperature (LST) and is a major indicator and determinant of UHI (Kikona et al., 2016; Ali Jasim et al.; 2016, Bakhtiar and Thomas, 2013; Zhong et al., 2016; Yue and Xu, 2007; Kalnay and Cai, 2003).

Urbanization typically causes a removal of natural vegetation and replacement of same with impervious and non-evaporative urban materials with high heat capacity and low solar reflectivity, such as concrete masses, asphalt roads and metal surfaces (Farina, 2012). The alteration of the natural land cover due to urbanization causes a change in the thermal properties of the urban landscape, with the effect that the urban land surface typically has a relatively higher thermal capacity than that of rural areas, thereby increasing the urban surface temperature. Research interest in LST and UHI has been sustained by the growing economic, social, environmental, and health consequences of the UHI phenomenon. Given the current high rate of global urbanization, UHI and its potential impacts are estimated to affect a large number of the world population, especially in the developing countries where the rate of urbanization is notably high (Jeppesen, 2013).

Early approaches to the study of UHI effects includes sampling of air temperature at different point locations using air samplers, thermometers, etc. (Smith et al., 2011; De Rezende et al., 2013; Ali Jasim et al., 2016), and the interpolation of the obtained point data sets to generate a temperature surface for a given area of interest. More recently, however, space-borne remotely sensed imagery have been widely used to understand the thermal, biophysical and the general environmental conditions on or near the Earth surface (Lu et al., 2015; Bakhtiar and Thomas, 2013; Zhong et al., 2016; Yue and Xu, 2007).

When studying UHI using a remote sensing approach, LST is the entry point, as well as a key parameter. This is because LST is closely related to UHI and hence LST provides the needed insight into the general UHI conditions. In addition, “space-borne sensors do not directly measure canopy air temperatures (which may represent urban heat Island) but measure land

surface temperatures" (Wang et al., 2016), through which UHI can be estimated. For more than three decades until now, studies on the UHI effect using remote sensing have been conducted at multiple spatial and temporal scales, using different satellites- and sensor-derived products (Gallo and Owen, 1998; Streutker, 2002; 2003).

1.2 Relevance of Study

The impacts of global warming can be particularly pronounced or even exacerbated in cities due, in part, to the UHI effects and the unique socioeconomic character of the urban environments. Extant literature documents consequences of extreme heat events on human health, physical infrastructure, animals and the general wellbeing of urban dwellers (Kovats & Ebi , 2005, Withman et al, 2006). With a projected 4^{o}C rise in average annual global temperature in the nearest future (Martinez-Austria, et al; 2018) and given the rapidly increasing rate of urbanization especially in the developing world, it becomes pertinent to understand the complex processes and factors driving the UHI phenomenon and to characterize the exact trajectories by which the heterogenous urban LCLU impact the UHI phenomenon.

Studies have shown that, in the last few decades, Ilorin city has undergone significant changes in landscape, population structure and urban form (Ibrahim et al., 2014; Olaleye et al., 2012; Olanrewaju, 2009). Olaleye et al. (2012) show that there is a decrease in vegetative land cover and a rapid increase in built-up areas in the city between 1986 and 2006, with a high potential for further reduction in vegetation land cover. In a similar study, Olanrewaju (2009) has confirmed a rising temperature in Ilorin in the last few decades. In addition, the city has been hit many times by heat waves with impacts sweeping across the urban population

including the animals. In 2012, Meteorological Organization projected that Nigeria, including Ilorin, would continue to experience elevated temperatures especially during the dry seasons (NIMet, 2012). Nigerian Meteorologists and epidemiologists have also warned of possible outbreak of some diseases that thrive in hot weather such as meningitis, tuberculosis, malaria, dengue fever, measles, chicken pox, skin rashes, and heart attack (Ahmed, 2012). As typical of many cities in Nigeria, energy generation in Ilorin is grossly inadequate and unstable and a greater majority of the population cannot afford air conditioners plus the energy required to run it. There is little or no coordinated approach for managing the consequences of rising temperature; the medical facilities are either ill-equipped or non-existent. This prevailing condition reduces adaptive capacity of the city dwellers to the actual and potential impacts of UHI in the city.

Despite the availability of studies analyzing the spatial and temporal growth of the city and its land cover dynamics, there is yet little understanding about the link between Ilorin's urbanization-induced land cover change and the spatiotemporal pattern of LST and UHI in the study area. This study attempts to fill this knowledge gap. The research is framed within the context of finding a scientifically informed basis for an urban environmental quality intervention in the management of urban heat island in Ilorin.

1.3 Study Aim and Objectives

Specifically, the current study seeks to examine the possible impact of LCLU change and topography of Ilorin on the urban land surface temperature (LST) of the city and estimates the UHI index

for the study area from the period of 2000 to 2016. The following research questions were pursued:

1. What patterns exist in Land Surface Temperature (LST) in Ilorin in the period 2000 - 2016?

2. To what extent can vegetation cover measured via NDVI explain the patterns in LST observed in Ilorin between the years 2000 - 2016?

3. To what extent can the terrain elevation/topography of the study area account for the spatial pattern of LST in Ilorin?

4. Is there any significant difference in LST between the, urban and rural areas, between the wet and dry seasons and between the period of 2000 and 2016?

5. What is the possible magnitude of urban heat island in Ilorin within the period of 2000 to 2016

CHAPTER TWO

2.0 Literature Review

Given the rapid rate of global urbanization and its socioeconomic, environmental and health implications, it is not surprising that many studies have focused on the linkages between the urbanization process, especially urbanization-induced land cover changes, and urban biophysical conditions, as well as their implications for the health of urban dwellers (Population Bulletin, 2007). As a result of the heterogeneous nature of urban land cover materials, complex biophysical processes operate in the urban space, often in a circularly causal manner, to produce the observed urban thermal conditions including the UHI pattern. Urban surface temperature pattern is significantly driven by land cover materials (Bokaie et al., 2015). Land cover modifications due to urbanization affect urban microclimate in many ways, one of which is the formation of the UHI phenomenon (Lu et al., 2015; Zhong et al., 2016). UHI is arguably one of the most studied consequences of urbanization, often linked to LCLU change due to urbanization.

LST research has been approached from various perspectives, and continues to occupy the attention of the scientific community, in general, and environmental and urban planning professionals, in particular. In this section, existing literature relating to LST and its estimation approaches, its relationships with LULC and UHI, are reviewed. Also, the concept of UHI, in relation to LST, is examined.

2.1 Land Surface Temperature and the Urban Heat Island Phenomenon

LST is an entry point and a key parameter in the study of UHI when the remote sensing approach to UHI studies is adopted. While LST studies have focused on different objectives, several studies of LST have focused on the UHI phenomenon, and particularly, its spatial and temporal characteristics (Oke, 1982; Lu et al., 2015; Bakhtiar and Thomas, 2013; Zhong et al., 2016; Yue and Xu, 2007). The UHI phenomenon describes the relatively warmer condition of the urban environment as compared to its rural surroundings (Oke, 1982; Kaveh et al., 2016). Geer (1996), as cited in Farina (2012), describes the UHI as an 'island of heat' when compared with its rural surrounding with lower surface temperatures. Gill et al. (2007) show that the elevated surface temperature observed in the urban areas results from the nature of the urban land cover materials which are essentially impervious, heat-absorbing and non-evaporative, thus making urban landscapes relatively warmer than their surrounding rural areas. In addition to the land cover effect on UHI, increased industrial, vehicular, and related anthropogenic activities contribute to rising ambient temperature in the urban areas.

Yuan and Bauer (2007) categorized UHI into three types, namely: Canopy Layer Heat Islands (CLHI), Boundary Layer Heat Islands (BLHI) and Surface Layer Urban Heat Island (SUHI). Both CLHI and BLHI, known together as atmospheric urban heat island (Grover and Singh, 2014), are described using above ground temperatures, about 1 meter from the ground surface (Farina, 2012), and can be measured via traditional network of weather stations (Yuan and Bauer, 2006). SUHI, however, is described as the temperature of the urban surface or urban land cover. Due to wind flow and the heat conductive capacity of the air, energy and heat from the Earth surface can be transferred to the air above it, such that SUHI may sometimes extend vertically upwards

to reach some meters above the ground, especially at night. SUHI is essentially the phenomenon that is experienced by urban dwellers as UHI.

Land Surface Temperature (LST), on the other hand, is the radiative skin temperature of the land surface, as measured in the direction of the remote sensor (Copernicus Global Land Service, 2017). In general, LST is measured using infrared remote sensing. LST is closely related to SUHI, as the energy or heat emitted by a surface can permeate the air around or above it through various processes of heat transfer.

2.2 Relationship between Land Surface Temperature and Land Cover / Land Use

Urban environmental research is replete with studies on the impact of land cover / land use on urban LST (see Vogt and Oke, 2003; Rose and Devadas, 2009; Farina, 2012; Feng and Myint, 2015; Ching et al., 2016; Pal and Ziaul, 2016). Ching et al. (2016) investigated the diurnal LST variation of Taipei City using MODIS and SPOT multispectral images. Their study shows that diurnal LST increased with increasing urbanization, with a positive linear increase observed at the early stages of urbanization. Pal and Ziaul (2016) assessed the impact of land use land cover on LST in English Bazar Municipality of Maldal District, India. Their findings confirm that LST varies spatially and with seasons, with impervious and built-up surfaces showing high LST values. In a related study, Feng and Myint (2016) explored the effect of neighboring land cover pattern on land surface temperature of central building objects. In their study, buildings were categorized into low-rise, mid-rise and high-rise buildings, and the land cover composition surrounding the building spaces was included in the analysis of the LST pattern. The results of

that study show that the composition of the land cover features surrounding the buildings has an effect on building LST. Rahman et al. (2017) confirm a positive high correlation between built-up areas and rising LST values.

Farina (2012) assessed the relationship between vegetation types and LST in the city of Seville, Spain. Using NDVI as a proxy for vegetation cover, he reported a negative relationship between vegetation cover and LST. Even though the NDVI-LST relationship was generally found to be negative, it was observed that some vegetation cover types were more influential than others in determining the LST characteristics of an area.

In China, various studies have investigated the temporal and spatial pattern of LST in relation to the composition and changes in LULC. For instance, Rasul and Ibrahim (2017) examined the changes in land use / land cover pattern and their impacts on the intensity and spatial pattern of UHI in a rapidly changing area of China. Using various land cover parameters such as Normalized Difference Vegetation Index (NDVI), Normalized Difference Water Index (NDWI), Normalized Difference Barrenness Index (NDBal) and Normalized Difference Built-Up Index (NDBI), it was shown that correlations between NDVI, NDWI, NDBaI, and temperature are negative, especially when NDVI is limited in range. However, a positive correlation was observed between NDBI and temperature. Wang et al. (2016), Hong (2016), and Tyubee and Anyadike (2012) also confirmed a strong relationship between land cover and LST.

Beyond the impact of land cover composition on LST, recent studies have assessed the impact of the spatial configuration of land cover on the LST profile. For instance, Zhibin et al. (2014) examined the relationship between LST and urban vegetation configuration, and, in particular, whether the relationship changes across scales. The results suggest that not only

increasing the amounts of urban vegetation, but also optimizing their spatial pattern, can decrease LST.

2.3 Land Surface Temperature and Remote Sensing Technologies:

Until the advent of remote sensing technologies, urban meteorological studies have relied heavily on point sampling of air temperature at given geographic locations (Hung et al., 2006). Remote sensing techniques have proved to be more efficient in collecting land surface temperature data, given their ability to record spatially contiguous data over a large geographic space (Yue et al., 2007). Apart from operating at high spatial resolutions, increased frequencies of re-visit times (temporal resolution) of the sensors have enabled time-series analysis of the important biophysical process occurring on or near the Earth surface. Landsat Thematic Mapper/Enhanced Thematic Mapper Plus, Operational Land Imager (TM/ETM+, OLI), the Moderate Resolution Imaging Spectro-radiometer (MODIS), the Advanced Very High Resolution Radiometer (AVHRR), the Advanced Space-borne Thermal Emission and Reflection (ASTER), the Geostationary Operational Environmental Satellites (GOES), and Satellite Pour I'Observation de la Terre (SPOT) images have been extensively employed to analyze changes in surface temperature (Singh et al., 2014).

While remote sensing is renowned for acquiring spatially extensive data at relatively high temporal resolution, poor data quality and data retrieval issues are not uncommon. For instance, capturing data for some parts of the Earth using remote sensing, especially in the tropics, has proven difficult owing to high humidity and cloud cover challenges. Similarly, due to climate and weather-related factors, remotely sensed data from the tropics, for instance, are

either not available, incomplete, or simply unusable for most of many seasons. Dealing with satellite-based remotely sensed data quality has been complicated by data validation and sensor calibration problems. Li et al. (2013) has raised issues of possible errors in sensor calibrations and measurement and challenges that lurk within LST data validation. They observed that far fewer studies have been undertaken to validate the satellite-derived LSTs, due to the difficulty of making ground measurements of the LST that are representative at the satellite pixel scale. With the recent launch of Landsat 8, and Sentinel 1 and Sentinel 2, and the prospect of future advancements in space science and technology, however, LST data acquisition, retrieval and applications are expected to improve.

In Nigeria, there is a paucity of studies on the drivers and pattern of LST, especially in urban environments. Given the observed high rate of urbanization in Nigeria and Ilorin in particular (Ibrahim et al., 2014), the current study attempts to fill the knowledge gap in the land cover impacts on, and the spatial and temporal characteristics of, LST in Ilorin. The relevance of the current research derives from the need to estimate the possible impacts of climate change on the urban environments, especially in the face of threats posed by a potentially rising LST traceable to rapid urbanization. In the current study, cloud-free (less than 10% of cloud cover) Landsat scenes have been processed to obtain the LST and the NDVI data sets required for analysis. More details on the data and methods of analysis are provided in the methods and data section.

CHAPTER THREE

3.0 Data, Methods and Study Area

3.1 Data

The current study made use of remotely sensed data from LANDSAT. Specifically, Landsat data were used for land cover classification, calculation of NDVI, and for the retrieval of the Land Surface Temperature (LST). These data are available at United States Geological Survey (USGS) website. Pursuant to the objectives of the study, Landsat imagery from November 2000, April 2002, April 2016 and December 2016 for the wet and dry seasons were acquired. In the study area, the wet season spans the months of March to October, while the dry season lasts from November to February (see Table 1).

For terrain elevation analysis, a 12.5 m spatial resolution digital elevation model (DEM) was acquired from the Alaska Satellite Facility (ASF) (www.asf.alaska.edu). ASF Radiometrically Terrain Corrected (RTC) products are distributed at two resolutions, that is RT1 and RT2. RT1 product was utilized in the current project. The RT1 products have a pixel size of 12.5m achieved by up-resampling and are generated from high resolution (NED 13) and mid-resolution (SRTM 30 NED1 and NED2) DEMs. These products are terrain-corrected at the native pixel size of the DEM that is used for the correction. ASF DEM has vertical accuracy of 4.85 meters. The accuracy of the various DEM sources was analyzed by Gesch et al (2014), comparing the DEM with reference data in the form of the National Geodetic Survey (NGS). All RTC products are geocoded to the Universal Mercator (UTM) projection and provided as floating--point power values in GeoTIFF format.

Table 1: Description of Landsat Data

Landsat	*Sensor*	*Acquisition Date*	*Path/Row*	*Spatial Resolution*	*Cloud Cover*
LandSat 7	ETM+	April, 2002	190/54	30/60* m	1%
		November, 2000			4%
LandSat 8	OLI	April, 2016.	190/54	30/100* m	5%
		December, 2016.			0%

(*Thermal Infrared bands were resampled to 30 meters for both sensors)

The administrative boundary polygon of Ilorin was downloaded from ESRI Living Atlas and the polygon was used to visualize the study area on ESRI-ArcGIS base map as well as to clip the Landsat data for further analysis. Red Green Blue (RGB) bands of Landsat were composited and was used for land cover mapping. The LCLU classification was validated with high resolution data obtained from Google Earth imagery.

3.2 Methods

3.2.1 Data Pre-processing:

Landsat Level-1 products were used in the current study. Landsat Level-1 products are precision registered and orthorectified through a systematic process that involves ground control points and a digital elevation model (DEM). The Landsat Level-1 products are termed "terrain-corrected" and the images can be used as delivered by the USGS (2015c). As such no geometric corrections were applied to the Landsat used for the study area. Dark Object Subtraction-1 (DOS-1) method of atmospheric correction was applied to all the thermal bands and bands 3 and 4 and 4 and 5 of the ETM+ and OLI sensors respectively. This correction was implemented using Semi-automatic Classification plugin in QGIS. In DOS-1 method, elements

such as water body and shadows are considered dark objects when their values of reflectance are close to zero and these objects are detected automatically when the pixel reflectance value is less or equal to 1.0% (Jesus et al, 2018). All bands were resampled to 30 meters spatial resolution.

3.2.2 Data Processing

3.2.3 Land Cover Map and the Normalized Difference Vegetation Index (NDVI)

To investigate the change in land cover within the period of 2000 to 2016 in the study area, the land cover maps for the wet season (April) of the two years (2002 and 2016) were computed. It was reasonable to map the landcover of the study area using the imageries for the wet season since the contrast among the land cover classes of interest would be more accentuated during this period, during which the vegetation would be greener and water bodies fuller and hence aid in potentially characterizing the different land cover types. Land use land cover classes of interest are built-up/bare ground, forest vegetation, grass/sparse vegetation, and water bodies. For the land cover maps, a semi-supervised classification method and the Maximum Likelihood Classification Algorithm (MLCA) were used. A semi-supervised classification method involves, first, using a non-supervised method to classify the pixels into a given number of clusters, followed by the use of training data to assign the pixels into different land cover classes. An average of 25 training samples was used for each of the land cover classes.

NDVI of both wet and dry seasons for both years (2002 and 2016) and seasons (wet and dry) were computed using the red (0.63-0.69 μm) and near-infra red (0.75-0.90 μm) bands of the ETM+ data sets. Also, equivalent bands (bands 4 and 5) were used to compute NDVI for wet

and dry seasons of 2002 and 2016 from OLI images. Detailed steps for deriving the NDVI is contained in the appendix 1. Land surface temperature was computed from LANDSAT 7ETM+ and LANDSAT 8 OLI images used in the study.

3.2.4 Land Surface Temperature (LST) Estimation (LANDSAT 7 ETM+)

Step 1:

3.2.4.1 Conversion of Digital Number (DN) to TOA Spectral Radiance:

The Digital Numbers of Landsat 7 ETM+ were converted to spectral radiance using the formula below as provided in *Landsat 7 Hand Book (2001), pg. 117-118* .

Lλ = ((LMAXλ - LMINλ)/(QCALMAX-QCALMIN)) * (QCAL-QCALMIN) + LMINλ (Equation 1)

Where: ***Lλ*** = Spectral Radiance at the sensor's aperture in watts/(meter squared * ster * μm)

QCAL = the quantized calibrated pixel value in DN

LMINλ = the spectral radiance that is scaled to QCALMIN in watts/(meter squared * ster * μm)

LMAXλ = the spectral radiance that is scaled to QCALMAX in watts/(meter squared * ster * μm)

QCALMIN = the minimum quantized calibrated pixel value (corresponding to LMINλ) in DN

= 1 for LPGS products

= 1 for NLAPS products processed after 4/4/2004

= 0 for NLAPS products processed before 4/5/2004

QCALMAX = the maximum quantized calibrated pixel value (corresponding to LMAXλ) in DN = 255

Step 2:

3.2.4.2 Conversion of Spectral Radiance to Radiant Surface Temperature:

For the ETM+ sensor (ie. 2000 and 2002 images), band 6 was converted from spectral radiance (as obtained in Equation 1 above) to radiant surface temperature using the equation 4 as provided by the *Landsat Project Office (2001), pg. 120*:

TB = K2/ (ln(K1/ Lλ + 1)) (Equation 2)

Where: TB is radiant surface temperature (in Kelvin);

K2 is calibration constant 2;

K1 is calibration constant 1;

Lλ is the TOA spectral radiance

3.2.4.3 Land Surface Temperature (LST) Estimation (LANDSAT 8 OLI)

For Landsat 8 TIRS scenes, the steps to estimate LST are similar to the ETM+ images. See Landsat 8 Data Users Hand Book (2016).

LST = TB / (1 + (λ TB / ρ) lnε. (Equation 3)

Where: LST is land surface temperature (in Kelvin);

TB is radiant surface temperature (in Kelvin);

λ is the wavelength of emitted radiance (11.5 µm);

ρ is h×c/σ (1.438×10 −2 m K);

h is Planck's constant (6.26×10-34J s);

c is the velocity of light (2.998×108 m/sec);

σ is Stefan Boltzmann's constant (1.38×10 -23J K-1); and

ε is emissivity. In sum ρ = 14,380.

Step 1:

3.2.4.4 Conversion of Digital Numbers to TOA Spectral Radiance

The value of Top of Atmosphere (TOA) spectral radiance (Lλ) was determined by multiplying band specific multiplicative rescaling factor of TIR bands with its corresponding TIR band and adding band specific additive rescaling factor to it using the formula

Lλ = M L*Qcal + A (Equation 4).

Where: *Lλ* is Top of Atmospheric Radiance in watts/ (m2*srad*µm)

ML is Band specific multiplicative rescaling factor (radiance_mult_band_10)

Qcal is- band 10 image value.

AL is Band specific additive rescaling factor (radiance_add_band_10)

Step 2:

3.2.4.5 Convert TOA spectral Radiance to Radiant temperature

Converting TOA spectral radiance to radiant temperature is achieved by applying equation 3 above. Because only band 10 of the Landsat 8 images was used,

ML and *AL* values for band 10 are 0.000342 and 0.1 respectively.

In all cases, emissivity parameters were applied using the formula in appendix 1b

3.3 Analysis of Spatial Pattern of LST in the Study Area

A spatial statistical approach was necessary to understand the spatial pattern of LST in the study area. So, a spatial autocorrelation analysis was conducted for the four different scenarios (all season and years) using the spatial autocorrelation (SA) tool in ArcGIS 10.5.1. The results of the SA characterize the spatial pattern of the LST for the different seasons and all the years for the study area. The spatial autocorrelation (Global Moran's I) tool measures spatial autocorrelation of a feature by simultaneously considering both the features' location and the attribute of the feature. In the current study, the spatial autocorrelation of LST was estimated by simultaneously considering both the location of the LST points and the attribute (value) of the point to determine whether the pattern expressed is clustered, dispersed, or random. The tool calculates the Moran's I Index value, and both a z-score and p-value to evaluate the significance of that Index. P-values are numerical approximations of the area under the curve

for a known distribution, limited by the test statistic (ESRI ArcGIS 10.5.1 Help). This was summarized using summary statistics for all the seasons and years.

3.3.1 Urban Heat Island Intensity

UHI intensity is an important parameter that provides insight into the temperature difference between the urban LCLU and the surrounding non-urban area. Specifically, the UHI intensity can be defined as the difference between area-averaged urban temperature and the area-averaged temperature of the surrounding non-urban/rural LCLU. The UHI intensity can be calculated using the equation 5 below.

$$UHII = T^{U} - T^{R} \quad \text{(equation 6)}$$

where **UHII** is the Urban Heat Island Intensity, $\mathbf{T^U}$ is the area-averaged temperature of all urban pixels, and $\mathbf{T^R}$ is the area-averaged temperature of all non-urban/rural pixels

To understand the magnitude of the UHI in the study area within the period under consideration, the study area was broadly classified into urban and non-urban LCLU. Because urban periphery can be significantly heterogenous in terms of LCLU as it could contain a mixture of urban and non-urban pixels, pixels at the urban periphery were removed to avoid biasing the UHI intensity estimation. Similarly, patches of urban LCLU were removed from areas broadly classified as non-urban. This is reasonable given the fact that UHI intensity is sensitive to and depends on which non-urban LCLU type(s) is selected for comparing with the urban areas (Mangelin, 2012). Hence LST for non-urban areas were retrieved from rural land cover types namely, forest/bushes, grasses/ sparse vegetation and water bodies within the non-urban area. Zonal statistics tool in ArcGIS was used to extract the mean LST of all the urban

pixels as well as the mean LST of all rural pixels. The UHI intensity was arrived at by calculating the mean difference between urban and non-urban LST for November 2000, April 2002, April 2016 and December 2016.

3.3.2 Relationship between Vegetation Cover and LST

A simple linear regression model was employed to characterize the relationship between LST and vegetation abundance measured via NDVI for each of the two seasons and the two periods (2000 and 2016). For each season, a randomly chosen set of 16,922 samples points (2% of the total pixel counts) in the study area was used for the regression analysis between NDVI and the LST values. NDVI is used as the independent variable while LST is the dependent variable. The adjusted R^2 (coefficient of determination) and the slope of the regression model, respectively, describe the percentage of the variation in LST accounted for by NDVI and the direction of the relationship between the 2 variables.

3.3.3 Relationship between Elevation and LST

In order to examine the possible relationship between topography and LST in the study area, terrain elevation values were regressed against corresponding LST values in each of the seasons and years using same sample points as in NDVI-LST regression. The analysis was achieved using a simple linear regression model.

3.3.4 Difference in LST between the Season and the Years

To examine if there is a significant difference between the LST values in the 16-year interval (2000-2016) and between the seasons (wet and dry) in the study area, paired t-tests were conducted using same sample points as in above. Pairs were constructed between seasons and between years.

3.4 The Study Area

3.4.1 Geographical Setting

This research used a study area centered on Ilorin, the capital of Kwara State, Nigeria. The geospatial datasets cover a rectangular extent, reaching from latitudes 8° 24'N to 8°45'N and longitudes 4° 29'E to 4° 58'E (see Figure 1).

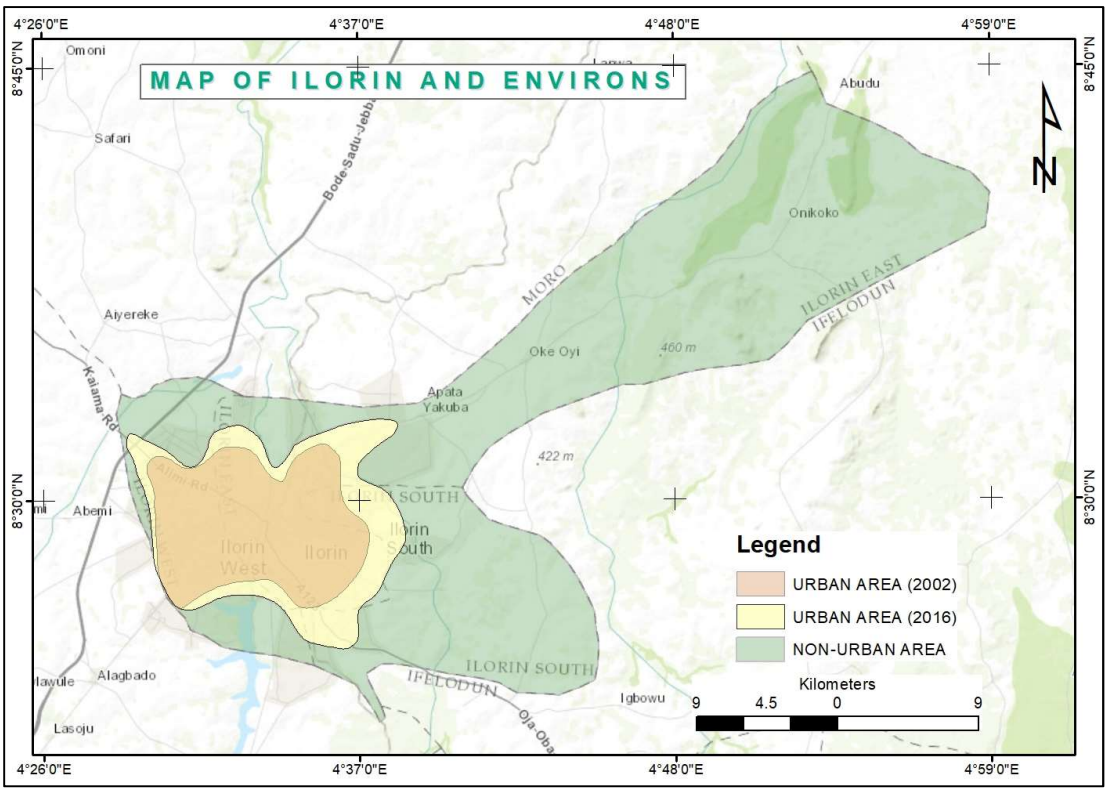

Figure 1: *Map of Ilorin (Study Area showing urbanized areas in 2002 and 2016)*

3.4.2 Climate, Vegetation, Relief and Soil:

Ilorin is located in a zone between the deciduous woodland of the South and the dry savanna of Northern Nigeria (Jimoh, 2003). The climate of Ilorin is characterized by wet and dry seasons, with temperatures ranging from 33° C to 34°C from November to January and 34°C to 53°C from February to April (Ilorin Atlas, 1982; as cited in Ajadi, et al., 2011).

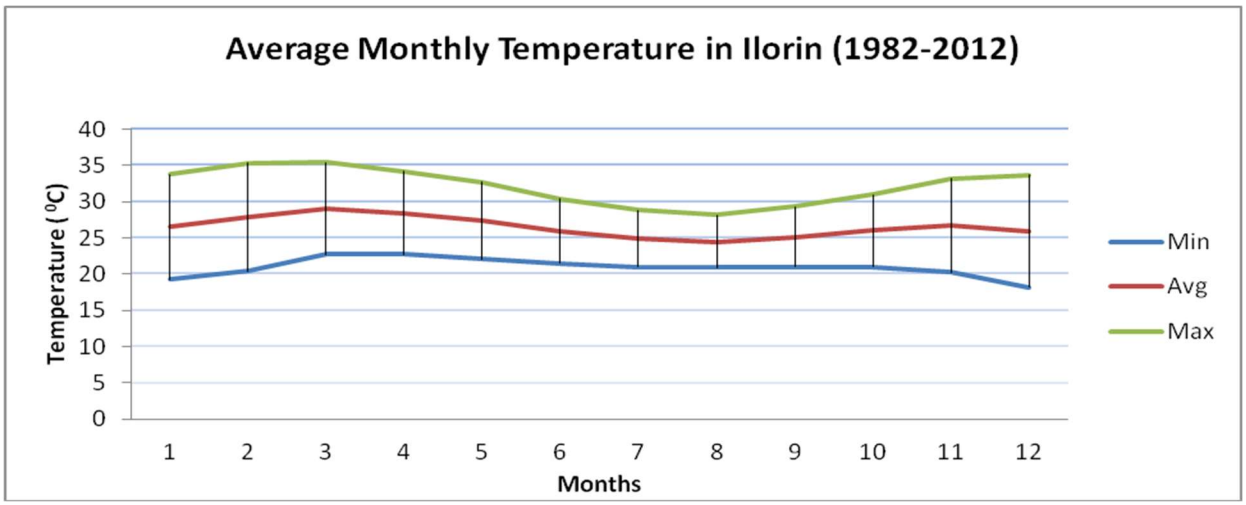

Figure 2: Average Monthly Temperature in Ilorin (1982- 2012) (Adapted from Climate Data.org-http://en.climate-data.org /location/538/)

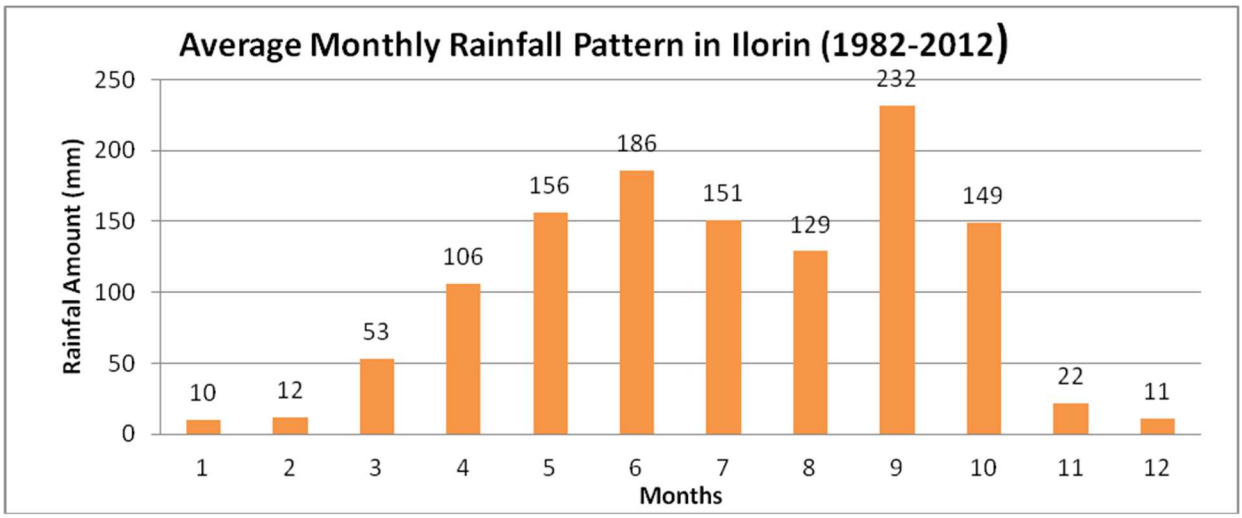

Figure 3: *Average Monthly Rainfall in Ilorin (1982- 2012) (Adapted from Climate Data.org-http://en.climate-data.org/location/538/)*

Rainfall in the city varies both spatially and temporally, with peaks between the months of March and October (Oyegun, 1987 ; as cited in Jimoh and Iroye, 2011). Especially during the dry season, Ilorin is characteristically sunny and hot in the day and warm at nights.

3.4.3 Urbanization

When urbanization is defined as the 'increased concentration of people in the urban areas rather than in rural areas' (UN-Habitat, 2006), it could be said that Ilorin's urbanization started before the 19th century (Olorunfemi and Raheem, 2013). For instance, the population of the city was about 36,000 in 1911 (Ibrahim, et al., 2014) and has gradually grown to 2,365,000 in 2006 (see NPC, 2006). Like many other cities that emerged around same period in Nigeria, Ilorin retains the characteristics of traditional town alongside a modern urban center (Ajadi and Tunde, 2010). Plate 1 shows a section of Ilorin urban center along the overhead bridge.

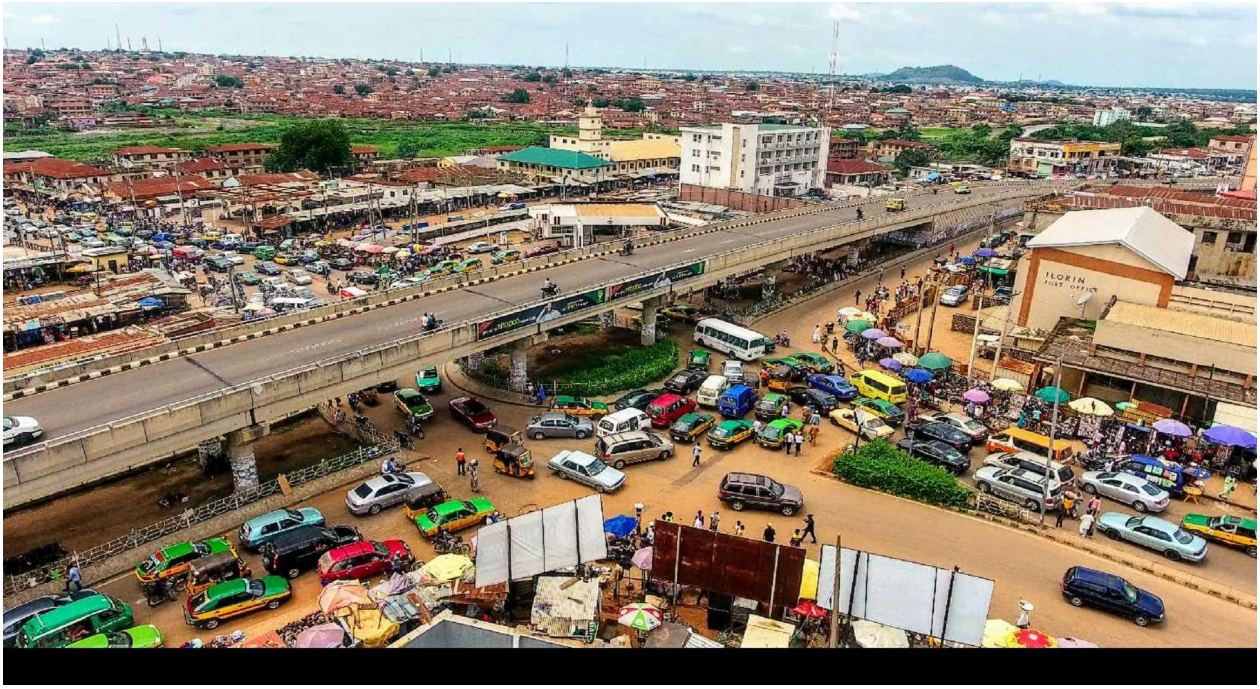

Plate 1: *A bird's eye view of Ilorin City from the side of the overpass bridge. Ilorin city structure comprises of different development zones /pattern evident in the type of building and infrastructure*.

Ajadi and Tunde (2012) have classified Ilorin urban structure and pattern into four different zones. Emir's palace, Central mosque and Emir's market have been identified as the central part of the city. This is followed by the zone of transition, which contain deteriorating houses. The third and fourth zones are concentrically organized around the second zone and are for the working-class residents and second-generation immigrants into the city respectively. The rural area comprises an admixture of modern and ancient building typically separated from one another. The rural areas (see plate 2) have lower population density and a few modern infrastructures. Road density is low in the rural areas and there are fewer economic activities going on. As the rural areas surround the city, they serve as commuters' zone for especially those who work within the urban periphery who find life lin the rural setting ess expensive than the urban core.

Plate 2*: Rural setting in Ilorin Area. This comprises of typically spatially separated buildings surrounded with natural vegetation and typically low grade access roads*

3.4.4 Population Growth Trend:

For a long time, the city's population did not show any appreciable growth, as it grew by only 4,000 inhabitants in 42 years, i.e. from 1911 - 1953 (see Figure 4). However, Ilorin has witnessed a significant growth, both in areal extent and in human population since 1967, when Kwara State was created, and Ilorin was designated as the administrative capital. Ilorin is currently an administrative and commercial hub of Kwara State and some settlements in surrounding states (Ibrahim et al., 2014). Mainly owing to this scenario, the city has become larger and more complex both in form and function, and consequently generates diverse environmental, social and economic impacts within and beyond its boundaries.

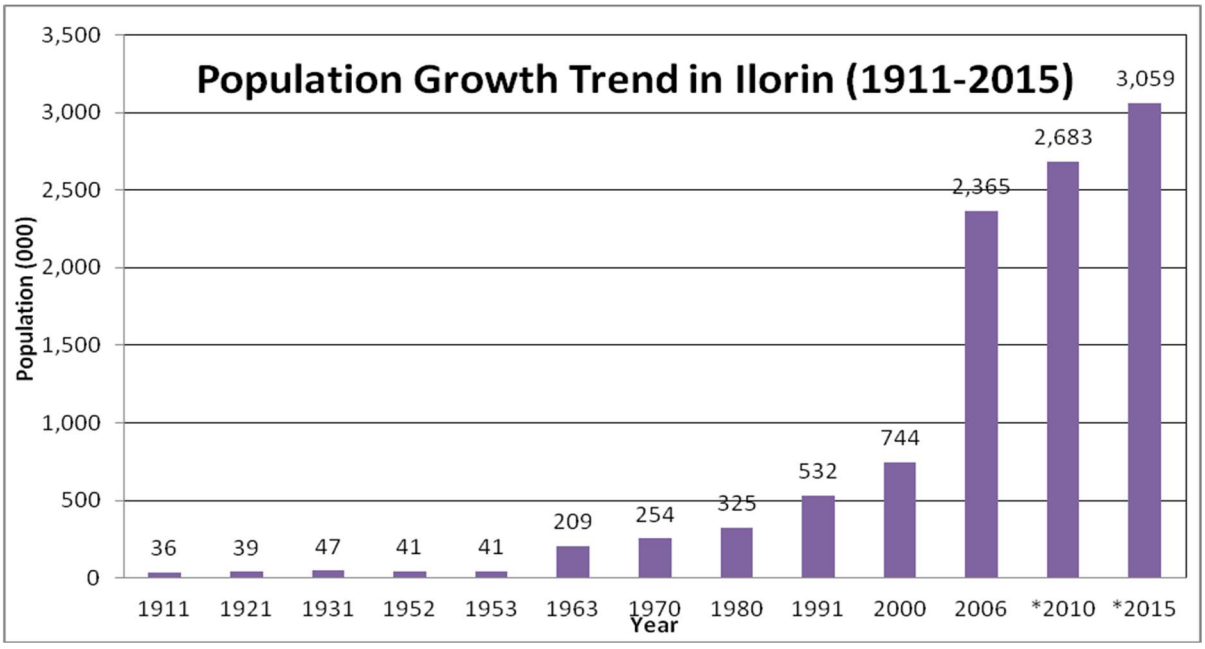

Figure 4: *Population Growth Trend in Ilorin. (Adapted from Ibrahim et al, 2014) (*projected)*

CHAPTER FOUR

4.0 Result and Discussion:

4.1 Spatial Distribution of Land Cover

Land Use/Land Cover: The results of the land cover classification and analysis for April 2002 and April 2016 are shown in Figure 5 and summarized in Table 2. Dense vegetation/forest and grassland/sparse vegetation were the dominant land cover types, and these accounted for 64% and 41%, and 26% and 46% of all the land cover types in 2002 and 2016, respectively. Built-up/bare ground had aerial extents of 73km^2 and 96km^2, representing 9.6% and 12.6% of the area in 2002 and 2016, respectively. The area of water bodies (notably the Assa River and Assa dam reservoir) remained relatively constant in area cover within the time period under study.

Table 2: Descriptive Statistics of Land cover classification of the Study Area for 2000 and 2016

	Area (km2)	Percentage (%) Cover	Area (km2)	Percentage (%) Cover
Built-Up/Bare Soil	73	9.6	95	12.6
Dense Vegetation/Trees	491	64	316	41
Grass/Farmland	196	26	349	46
Water Bodies	2.7	0.4	2.7	0.4
Total	**762.7**	**100**	**762.7**	**100**

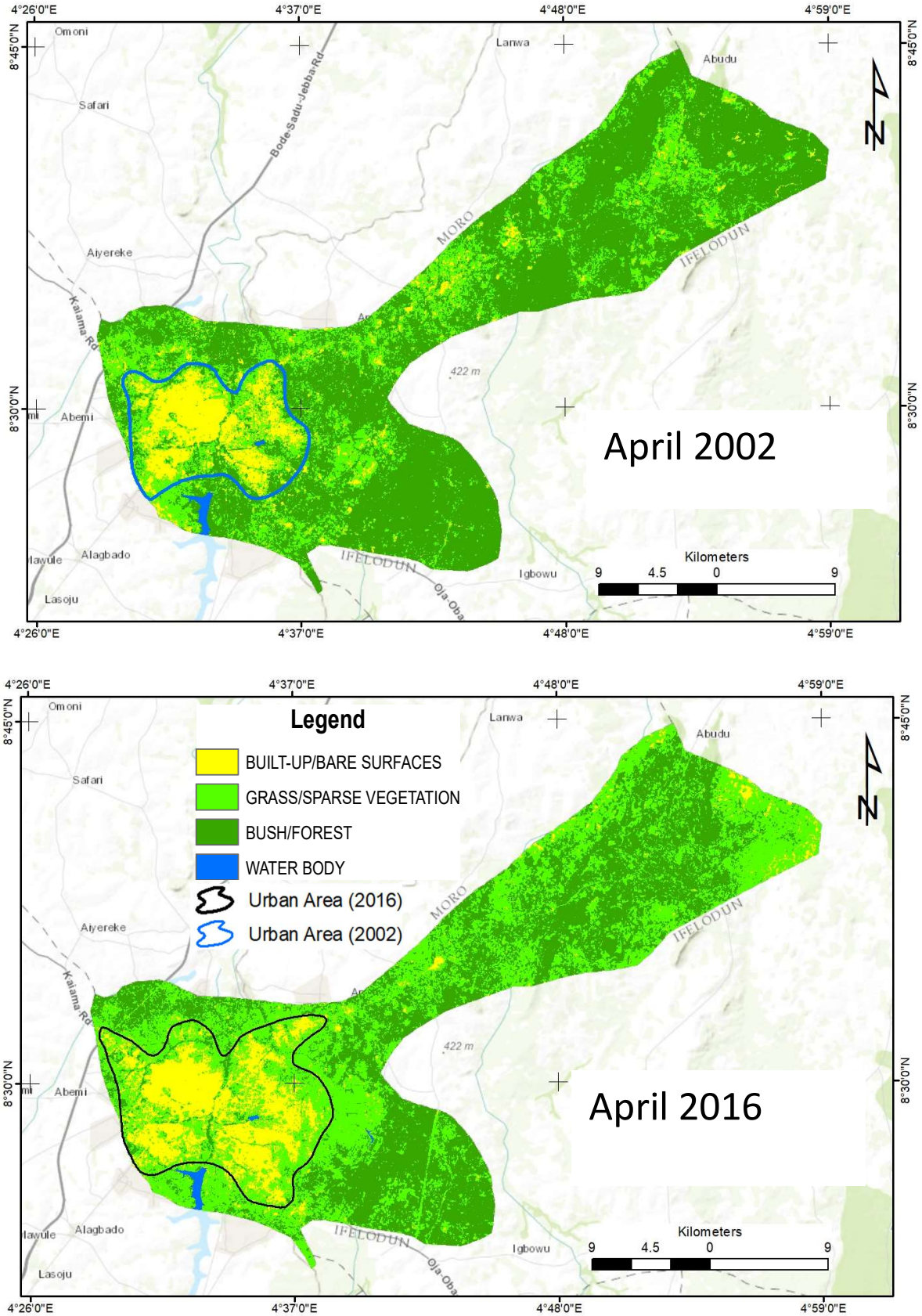

Figure 5: *Land cover classification for April 2002 and April 2016 showing various land cover classes and urban expansion within the period*

4.2 Spatial Pattern of Land Surface Temperature

Generally, the LST values varied in both space and time (seasons and years), with a high temperature region noticeable, especially, in the built-up areas and decreasing towards the urban periphery (see Figure 6). The urban core is dominated by high values of LST irrespective of the season. For the period under study and across the study area, minimum and maximum LST values of 19^{o}C and 38^{o}C were recorded in April 2002 and November 2002, respectively. The difference between the minimum and maximum temperature across the study area were 16^{o}C, 13^{o}C, 12^{o}C and 13^{o}C for April, 2002 (wet season), November, 2000 (dry season), April, 2016 (wet season), and December, 2016 (dry season), respectively. The highest and lowest surface temperature variability across the study area were recorded in November 2000 and April 2016 with a standard deviation of 1.5^{0}C and 0.9^{0}C respectively.

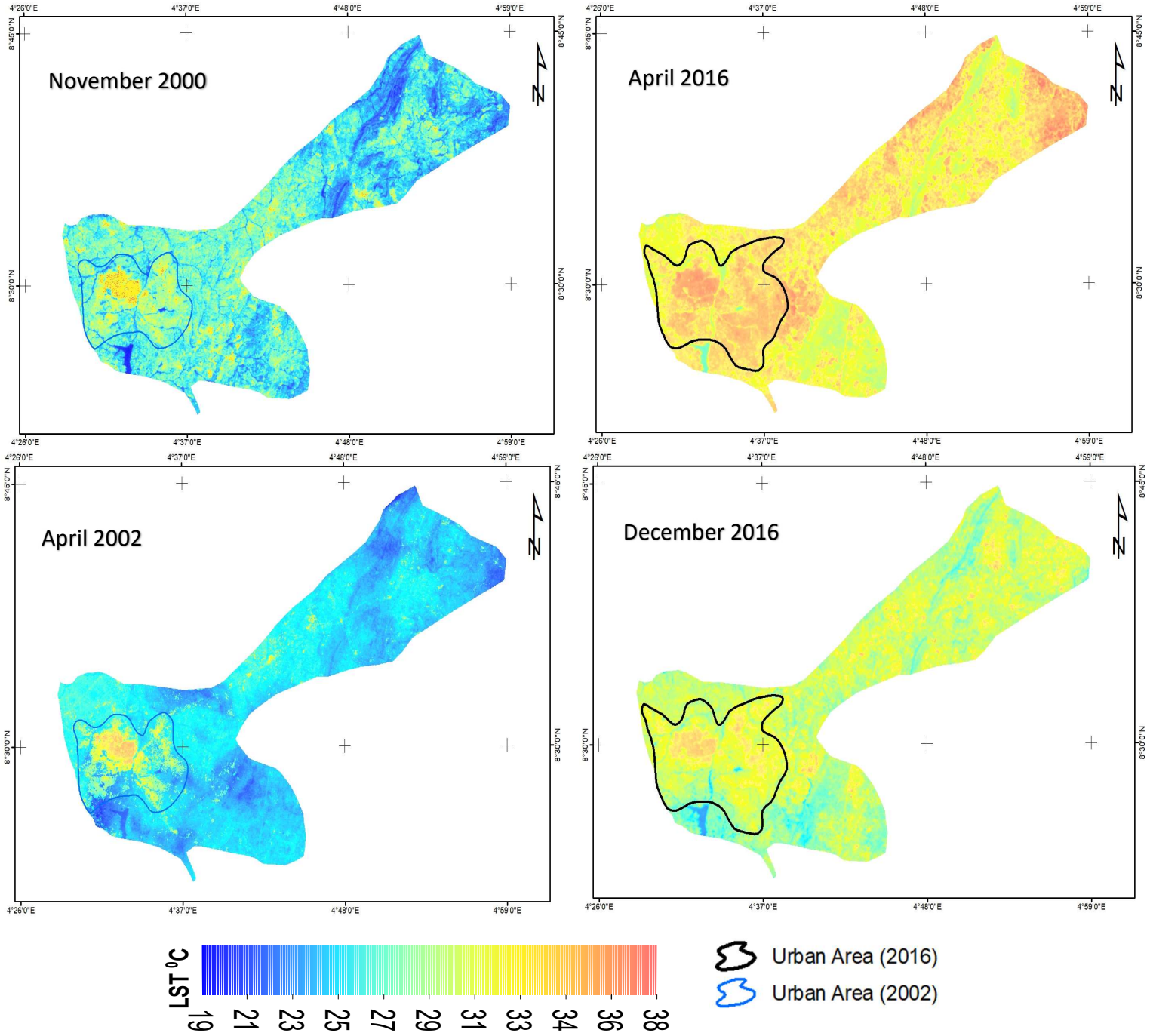

Figure 6: *Spatial Pattern of estimated LST for November 2000, April 2002, April 2016 and December 2016. The rings show the boundary of the urbanized/built up portions of the study area within the period under consideration*.

The spatial pattern of LST in the study was further quantitatively investigated using Global Moran's I statistic for spatial autocorrelation. The spatial autocorrelation analysis parameters / conceptualization used here are a fixed distance conceptualization, with a distance threshold / bandwidth of 500 meters, and the Euclidean distance method was applied.

The result of the Moran's I spatial autocorrelation analysis is shown in Table 3. The result of spatial autocorrelation analysis for all the seasons show positive Moran's I index values of greater than 0.6, z-scores of greater than 220 at $p < 0.001$. This suggests that there is a significant clustering of LST values in the study area. The observed positive spatial autocorrelation is for all the years and seasons in the study area. The result of the spatial autocorrelation analysis suggests that LST in the area may be driven by a certain underlying geographic process such as land cover type, etc.

Table 3: Spatial Autocorrelation Moran's I Result

Year/Season	Moran's Index	z-score	p-value
November 2000/ (Dry Season)	0.6	226.8	0.0000
April 2002/(Wet Season)	0.7	277.0	0.0000
April 2016/(Wet Season)	0.8	284.4	0.0000
December 2016/(Dry Season)	0.7	276.4	0.0000

4.3 Urban Heat Island Intensity

Figure 7 captures the trend of mean LST difference between the urban and rural pixels in the study area for all the considered epochs. In all cases, the mean temperature of urban pixels is higher than the non-urban areas. Mean urban LST varied over the years with an overall range of 3.9^0C, with the highest and lowest mean values recorded in 2002 and 2016. The wet seasons had the highest urban mean LST values across the study area. Mean urban LST fluctuated between 34^0C in 2002 and 30.1^0C in 2016 with a low-high, low-low trend within the four-time steps considered. The relatively higher range in the mean LST for urban pixels than the non-urban pixels signifies greater fluctuation in mean temperatures in the urban than the non-urban areas between the periods considered.

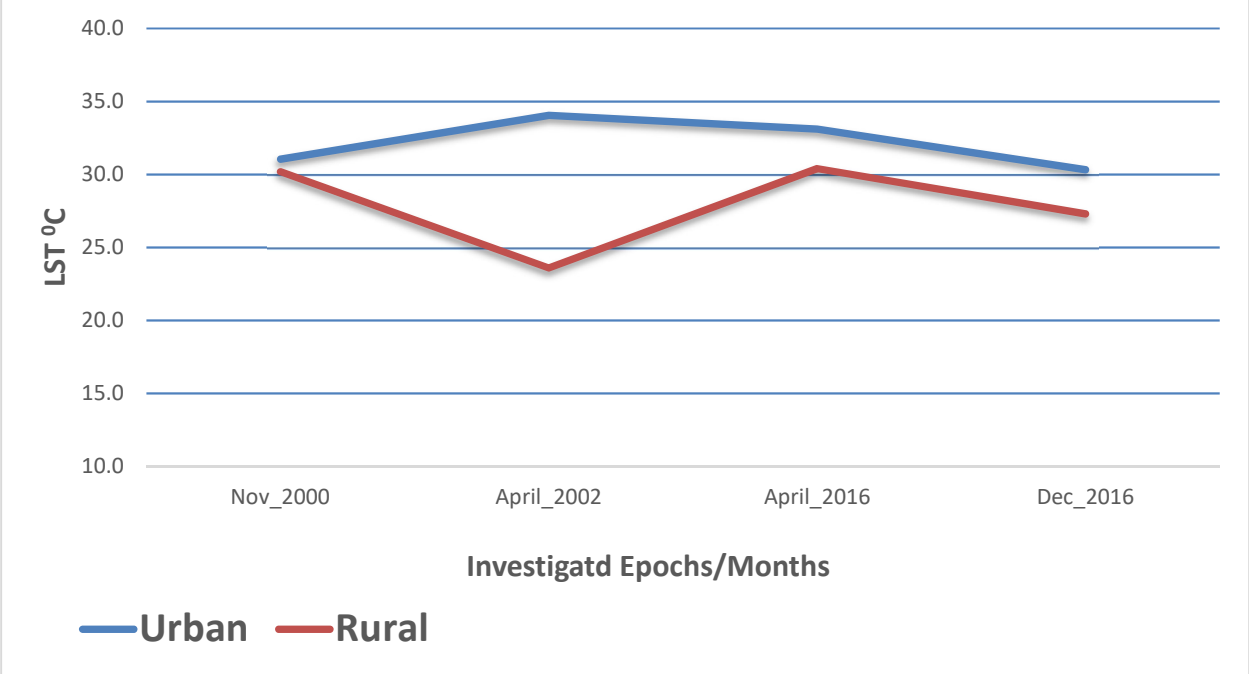

Figure 7: *Showing Mean of Urban – Rural LST in November 2000, April 2002, April 2016 and December 2016. The difference between the two lines of graph represents the magnitude of UHI within the investigated period.*

The difference between mean urban LST and the mean non-urban LST, that is, the UHI intensity, within the period varied between 0.2^0C to 4.6^0C. The highest magnitude of 4.6^0C was recorded in the wet seasons of April 2002 and April 2016. The dry season UHI intensity ranged from 0.2 to 1.0 in November 2000 and December 2016 respectively. The observed seasonal character of the UHI intensity where relatively higher UHI is observed in the wet than in the dry season may be linked to harmattan phenomenon. The harmattan is characterized by cold dry and dusty northeasterly trade wind that sweeps the West African subcontinent typically between the end of November and the middle of March. Harmattan phenomenon dominates the country including Ilorin around this period. Urban surface temperature can be moderated by the cold harmattan wind which keeps surfaces essentially cold and dry thereby lowering long wave radiation (sensible heat) from the LCLU surfaces that reaches the sensors onboard Landsat satellite.

4.4 Relationship between LST and NDVI

The relationship between LST and NDVI was investigated using an ordinary least square regression (OLS) model. Regression models were fit for the 2 different seasons (wet and dry) and for the 2 years to determine the influence of NDVI on LST. Two percent (16,922) of the total pixel counts of the image were randomly sampled from across the entire study area to run the analysis. For consistency purposes, and to allow for reasonable comparison, the same number and sample locations (pixels) were used for the analysis for all years and seasons. NDVI is the independent variable, while LST is the dependent variable. Table 7 shows the regression analysis

result for the study area, and for all the years and seasons. The coefficient for each independent variable reflects both the strength and type of relationship the independent variable has with

Table 4: Regression Analysis Result for LST and NDVI (* are significant at P < 0.001)

	Month/Year (Season)	Coefficient	Adjusted R-Squared
LST/NDVI	November /2000 (Dry Season)	-21.1*	0.7
	April /2002 (Wet Season)	-13.5*	0.4
	April /2016 (Wet Season)	-6.9*	0.5
	December /2016 (Dry Season)	-8.9*	0.3

the dependent variable. When the sign associated with the coefficient is negative, the relationship is negative (ArcGIS Help, ESRI 2017).

For all the seasons and years, the coefficients of the regression analysis results in the study area are negative indicating that NDVI is inversely related to LST. This suggests that the LST decreases with an increase in vegetation abundance. Regression coefficients were stronger in November 2000 and April 2002 with coefficients of -21 and -13 respectively. The predictive power of the models as indicated by the adjusted R is highest in November 2000 and April 2002, with adjusted *R* values of 0.7 and 0.4 respectively. The impact of NDVI on LST, as shown in the regression model, suggests that a change in NDVI or vegetation abundance of a given amount in November 2000 and April 2002 resulted in a more significant change in LST than on other dates. The year 2016 (April and December 2016) showed modest coefficients of -8.9 and -6.9, with adjusted R values of 0.49 and 0.29 respectively. All the coefficients are significant at $p < 0.001$.

4.5 Relationship between Elevation and LST

The spatiotemporal variation of LST as a function of elevation was also investigated using an ordinary least squares (OLS) regression model. A digital Elevation Model (DEM) with 12.5-meter spatial resolution with a vertical accuracy of 4.85 meters was used in analyzing the relationship between terrain elevation and LST in the study area (Figure 8). Detail of the DEM is found in the data and methodology session of this paper. The elevation of the study area ranges

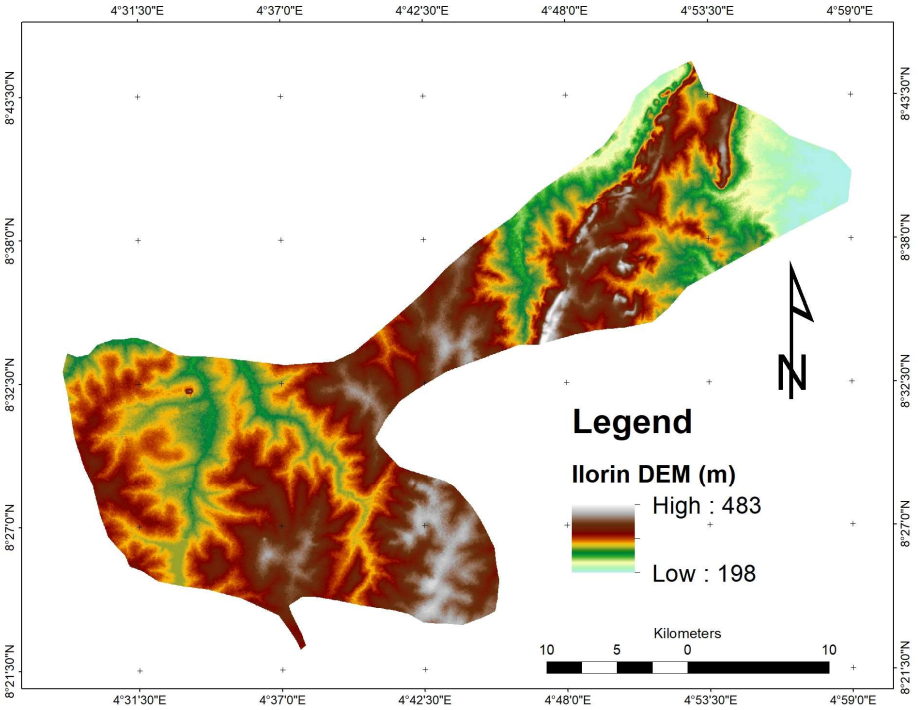

Figure 8: Digital Elevation Model of Ilorin

from 198 meters to 483 meters. The DEM was resampled to a spatial resolution of 30 meters to match LST raster layers using the nearest neighbor algorithm in ArcGIS. Nearest neighbor is a local interpolation method using only a subset of samples that surround a query point and interpolated values are guaranteed to be within the range of the samples used. It does not infer trends and will not produce peaks, pits, ridges, or valleys that are not already represented by

the input samples (ArcGIS 10.5 Help). Two percent (16,922) of the total pixel counts (same sample location as was used in NDVI-LST regression model) were sampled and analyzed, where LST is the dependent variable and the elevation was the independent variable. Table 5 shows the results of the regression model between elevation and the LST in the study area.

Table 5: Regression Analysis Result for LST and NDVI (* are significant at P < 0.001)

	Month/Year (Season)	Coefficient	Adjusted R Squared
LST/ELEVATION	November 2000 (Dry Season)	0.002	0.004
	April 2002 (Wet Season)	-0.000*	0.000
	April 2016 (Wet Season)	-0.004*	0.043
	December 2016 (Dry Season)	-0.001*	0.006

The correlation between elevation and LST in the study area is described by the coefficient of the independent (elevation) variable. The regression coefficients for elevation for the November 2002, April 2002, April 2016 and December 2016 models are 0.0015, -0.0016, -0.0035 and -0.0013, respectively. A negative coefficient indicates an inverse relationship between elevation and LST dates during the period under study.

Apart from the November 200, all the coefficients are significant at P < 0.01 with adjusted R values varying from 0% to 4%.

The current study also sought to examine if there is a significant difference between the LST values in the 16-year interval (2000-2016) and between the seasons (wet and dry) in the study area. To this end, using 2% (16,922) of the total pixel counts for each of the LST data sets

and the Statistical Package for Social Sciences (SPSS 2017) software, a paired t-test was conducted to examine if there is a statistically significant mean differences between the 4 different sample epochs. Samples were paired between seasons (wet and dry) and between years (2000 and 2016). The results of the paired t-tests are summarized in Table 6

The results show that the differences in the means of the LST for the different seasons and years are statistically significantly ($p<0.001$, $t= 170$). April 2016 has the highest mean of 32.33 and April 2002 recorded the lowest mean of 24.83. Based on the analysis, it could be concluded that the LST in Ilorin during the period under review has shown a significant change.

Table 6: Result of the Paired t-Test

	LST PAIRS	95% Confidence Interval Of Upper	t	df	Sig. (2-tailed)
Pair 1	APRIL2016- APRIL 2002	7.468	481.1	16921	.000
Pair 2	NOV2000 - DEC2016	2.708	170.7	16921	.000
Pair 3	APRIL2002 - *NOV2000*	7.360	509.4	16921	.000
Pair 4	APRI2016 - DEC2016	2.766	269.5	16921	.000

4.6 Discussion

The land cover / land use pattern of Ilorin city was analyzed and several possible factors capable of affecting the LST of the study area were considered. The relationships between LST and NDVI and elevation were investigated. Also, the study attempted to understand if there is any significant difference between the LST values of the different years and seasons within the temporal design of the study. As a significant factor affecting LST, and urban environment

temperature generally, the current study shows that land use land cover pattern has significantly changed during the period of 2000 to 2016. The urban proportion of the landscape has notably shown a significant increase, and the vegetation land cover, especially the forest component, has diminished within the period.

This pattern of land use land cover dynamics has implications for LST. Several studies have established the inverse relationship existing between vegetation cover- frequently proxied by NDVI- and LST. Expectedly, the Ilorin urban core, with its high density of built infrastructure, recorded the highest mean temperature, and the LST decreases towards the urban periphery, reflecting the land cover land use pattern. While the maximum and the minimum values of LST did not significantly change in the study area within the period under study, the portion of the city with increased LST values has increased. This shows that, as urbanization increases, the portion of the city and population experiencing rising LST will increase, as the LST follows the land cover pattern in all the years and seasons investigated.

The spatial and temporal pattern of LST in the area showed a presence of UHI with an intensity ranging between $0.2^{O}C$ to $4.6^{O}C$, with peaks in the wet seasons. The observed magnitude of UHI in Ilorin can have multiple economic, health and environmental implications for the urban dwellers. For instance, UHI can worsen air quality conditions and stimulate extra demand for energy for cooling. Given a poverty level of more than 80% in the city (Kwara State Ministry of Planning and Economic Development (2012) and paucity of quality health infrastructure, high magnitudes of UHI can potentially worsen the economic status and public health of the urban dwellers.

However, since a greater number of persons is increasingly living in the urban area, the city provides a potential geographic unit for intervention targeted at reducing the total population potentially facing high temperatures.

A Spatial autocorrelation analysis shows that the LST pattern is clustered. The Global Moran's I index for all the scenarios showed high values, greater than 0.6 with z-scores greater than 220 in all cases at $p < 0.001$, which signifies a statistically significant clustering of LST values in all the investigated epochs. Historically, such clustering of high values of LST are precursors of persisting enclaves or pockets of high LSTs that may qualify as Surface Urban Heat Islands. Again, the observed clustering pattern also provides a suitable geographic unit for urban planning interventions aimed at managing LST in the city.

The relationship between NDVI and LST confirms a typical inverse relationship as found in related studies. The literature is replete with studies confirming an inverse relationship between NDVI and LST. The intent of this study was not to reconfirm the relationship between NDVI and LST, as this has been sufficiently documented in the existing literature (Farina, 2012; Feng and Myint, 2015; Ching et al., 2016; Pal and Ziaul, 2016), but rather to investigate how much of the explanation for LST pattern is provided by NDVI, and whether there is a trend to this explanation.

To this end, it was noted that NDVI explained between 50% - 71% of the variation in LST between 2000 to 2002, and NDVI increasingly diminished in importance as an explanatory variable for LST in 2016, where only 29% - 49% explanation was provided by this variable. This is suggestive of a decreasing function of NDVI as an explanatory variable for LST. Several reasons can be postulated for the variation in the strength of the observed relationship between NDVI

as an independent variable for LST over the years considered. For instance, several authors have shown that not only the presence but also the spatial arrangement of vegetation has impact on the cooling effect of vegetation land cover on the urban climate (Zhibin et al. 2014). As urbanization increases in Ilorin, the spatial configuration and partitioning of existing vegetation will dynamically change and will potentially impact on the LST character. Also, city size has been linked to the degree of UHI (Rybski and Kropp, 2017, Oke, 1972), and as such, as the size of the city increases, the relationship between LST and vegetation is expected to change. Local climatic factors such as exposure to insolation, wind pattern and time of day can as well account for the observed pattern. Similarly, although a regression analysis between elevation and LST in the study area showed a statistically significant negative relationship in 3 out of the 4 scenarios, the strength of the elevation as an explanatory variable of LST was very weak, varying from 0% to 4%. At the very best, this shows that elevation is not a significant factor influencing LST in the study area.

A paired t-test between the LST means of each of the 4 time periods was conducted to establish if there is any statistically significant difference between the LST means. The results of the paired t-tests (the details of which are found above in Table 6) show that the LST for each of the periods is statistically significantly different from each of the others. That means that each of the seasons and years exhibited significantly different central tendencies in LST. Pairs 1 and 2 and pairs 3 and 4 (as defined in Table 8) were used to test mean difference between years, and mean difference between seasons, respectively. So, apart from the spatial variation of LST across the study area, there was also a variation in the mean LST across time during the period under study.

CHAPTER 5

5.0 Conclusion:

The current research sought to investigate the possible impacts of urban vegetation and elevation on the LST of Ilorin. Also, an attempt was made to describe and understand the spatial and temporal characteristics of LST in the study area. Based on the analyses undertaken, it could be concluded that the LST of the area is clustered in space and varied in time within the temporal extent of this research. High LST values are found clustered around the built-up urban region, and then LST diminishes towards the urban periphery. A clustering of high LST values in urban areas versus relatively lower mean LST in the rural areas is indicative of UHI in the study area. LST in the study area closely followed the pattern of land use land cover, thereby reinforcing earlier results and confirming the relationship between urban LST with LULC.

The relationship between vegetation (measured via NDVI) and LST showed varying significance over time. The degree of explanation of LST provided by NDVI waned with time, varying from about 70% in 2000 to about 40% in 2016. The reasons for this have been hypothesized. Nevertheless, the observed relationship between NDVI and LST in the study area confirms that while NDVI has been shown in the literature to be a significant factor in driving LST (Quattrochi and Ridd, 1994), its level of importance may vary given other intervening factors such as city size, season, elevation, and other local factors. This is insightful when considering the possible use of urban vegetation to lower LST or manipulate the UHI phenomenon.

Although, the study found elevation to be statistically significant as an independent variable for LST, it could be concluded that, given the value of the regression coefficients recorded for elevation and their corresponding R^2, elevation cannot be regarded as an important

variable in explaining the LST pattern in the area. The paired t-test results show that the mean LST for the dry season (November/December) are lower than those for the wet season (April), indicating a relatively warmer surface temperature in the wet season. This aligns with the measured annual mean temperatures for Ilorin as shown in Figure 2.

The UHI intensity in Ilorin shows appreciable change over time, tending towards a decreasing trend. However, further studies with higher temporal resolution and longer temporal extent may be needed to validate the observed trend. Nevertheless, it is obvious that the urban landscape in the study area is averagely significantly warmer by more than 2^0C than the rural space. When coupled with the overall relative high temperature of the city especially during the wet seasons (averagely above 33^0C), it calls for a conscious plan to manage a potentially rising temperature and its potential impacts on health, economy and human comfort generally. The overall nature and configuration of future development and urbanization of the city coupled with its local climatic variables will determine the exact character of the future UHI in the city.

It is worthy of note, that while the current study has investigated the temporal and spatial pattern of LST in Ilorin as well as the relationship between NDVI, elevation and LST, the LST data used in the study represents only a snap shot of the scenario. Therefore, conclusions drawn on this study should be interpreted accordingly. To get a better picture of the spatial pattern and trend of the LST within the period of interest, the temporal resolution of the LST data could be further increased to fill data gaps, subject to the availability of suitable, cloud free imagery for the study area.

References:

1. Abdulrahman Mariam Oluwatosin (2014) Assessment of Urban Growth and its Consequences on Infrastructural Facilities in Ilorin East Local Government Area, Kwara State. Nigeria. A thesis submitted to the Dept. of Geography, FUT MINNA.
2. Ajadi B. S, and Tunde, A.M (2010) Spatial Variation in Solid Waste Composition and Management in Ilorin Metropolis, Nigeria. *J Hum Ecol, 32(2): 101-108 (2010)*
3. Ajadi, B. S., Adeniyi, A., & Afolabi, M. T. (2011). Impact of Climate on Urban Agriculture: Case Study of Ilorin City, Nigeria. Global Journal of Human Social *Applied Meteorology*, 36, 1117–1132. Global Journal of HUMAN SOCIAL SCIENCE Volume 12 Issue 6 Version 1.0 March 2012
4. Ahmed, Y.A, (2012) Potential Impacts of Climate Change on Waste Management in Ilorin City Nigeria.
5. Bakhtiar, F., & Thomas, B. (2013) Examining Urban Heat Island Relations to Land Use and Air Pollution: Multiple Endmember Spectral Mixture Analysis for Thermal Remote Sensing. *IEEE Journal Of Selected Topics In Applied Earth Observations And Remote Sensing*, VOL. 6, NO. 3, JUNE 2013
6. Copernicus Global Land Service (2017). Land Surface Temperature. http://land.copernicus.eu/global/products/lst. Accessed 05/10/2017.
7. De-Rezende, C., Maciel M. K., Marta, C. (2013). The impact of surface characteristics on ambient temperature at urban micro scale: comparative field study in two climates. *International Journal of Low-Carbon Technologies 2015, 10, 165–175*
8. Kaveh, D., Kamruzzaman, M., & Hayes, J. F. (2016) Correlation or Causality between Land Cover Patterns and the Urban Heat Island Effect? Evidence from Brisbane, Australia.
9. Dongmei, L., Kaishan, S., Shuying, Z., Mingming, J., Jia, D., & Chunying, R. (2015). The Effect of Urban Expansion on Urban Surface Temperature in Shenyang, China: an Analysis with Landsat Imagery. *Environ Model Assess* (2015) 20:197–210 DOI 10.1007/s10666-014-9426-2
10. Farina, A. (2012): Exploring the Relationship between Land Surface Temperature and Vegetation Abundance for Urban Heat Island Mitigation In Seville, Spain. Master's Thesis Submitted to Lund University, Department of Geography and Ecosystem Analysis. LUMA-GIS Thesis Series 15
11. Feng, X., & Myint, S. (2016) Exploring the effect of neighboring land cover pattern on land surface temperature of central building objects. Building and Environment 95 (2016)
12. Gallo, K. P. & Owen, T. W. (1998). Assessment of urban heat island: A multi-sensor perspective for the Dallas-Ft. Worth, USA region. *Geocarto International*, 13, 35 – 41.
13. Gill, S.E., Handley, J.F., Ennos, A.R., & Pauleit, S. (2007). Adapting Cities for Climate Change: The Role of the Green Infrastructure. *Built Environment*, 33, 115-113
14. Ibrahim, R. B., Bako, A. I., Raheem, W. M., & Abdulyekeen, A. O. (2014) Appraissal of Urbanization Trends in Ilorin, Nigeria. *Journal of Sustainable Development in Africa* (Volume 16, No 8)

15. Kalnay, E. & Cai, M. (2003) Impact of urbanization and land-use change on climate. *Nature* 2003, 423, 528–531.
16. Li, P., Luguang, J., & Zhiming, F. (2014) Cross-Comparison of Vegetation Indices Derived from Landsat-7 Enhanced Thematic Mapper Plus (ETM+) and Landsat-8 Operational Land Imager (OLI) Sensors. *Remote Sens*. 2014, 6, 310-329; doi:10.3390/rs6010310
17. Jesus, A., Federico, V., Martin, M., Carlos, M., Eduardo, S and Alfredo, P (2018) Atmospheric and Radiometric Correction Algorithms for the Multitemporal Assessment of Grassland Productivity. *Remote Sens*. 2018, 10, 219; doi: 10.3390/re10020219
18. Liu, K., Hongbo, S., Xueke L., Weimin, W., Lijun, Y., & Hong, L.(2016) Quantifying Spatial–Temporal Pattern of Urban Heat Island in Beijing: An Improved Assessment Using Land Surface Temperature (LST) Time Series Observations From LANDSAT, MODIS, and Chinese New Satellite GaoFen-1, *IEEE Journal Of Selected Topics In Applied Earth Observations And Remote Sensing*, VOL. 9, NO. 5, MAY 2016
19. Olaleye, J. B. (2012), Land use and Land-cover Analysis of Ilorin Emirate Between 1986-2006, Using Landsat imageries. *African Journal of Environmental science and Technology*. Pg 189-198
20. Oyegun, R.O. (1987) Man-Induced Movement of Earth Materials into Ilorin City, Nigeria. Environmental Education and Information 6(2):142-152
21. Population Bulletin Volume 62 No 3, September (2007) http://www.prb.org/pdf07/62.3Highlights.pdf. Last Accessed 22/06/2017
22. Rahman, M.T., Adel, S. A., & Md, G. M. (2017) Modeling Future Land Cover Changes and Their Effects on the Land Surface Temperatures in the Saudi Arabian Eastern Coastal City of Dammam. *Land 2017, 6, 36*
23. Rasul, G & Ibrahim, F. (2017) Urban Land Use Land Cover Changes and Their Effect on Land Surface Temperature: Case Study Using Dohuk City in the Kurdistan Region of Iraq. Climate 2017, 5, 13; doi:10.3390/cli5010013
24. Rose, L.A., & Devadas, M.D., (2009). Analysis of and Surface Temperature and Land Use/ Land Cover Types Using Remote Sensing Imagery: A Case in Chennai City, India. Seventh International Confr. on Urban Climate, Japan.
25. Singh, R. B., Grover, A., & Zhan, J. (2014) Inter-Seasonal Variations of Surface Temperature in the Urbanized Environment of Delhi Using Landsat Thermal Data. Energies 2014, 7, 1811-1828; doi:10.3390/en7031811
26. Mehdi, B.M., Kheirkhah, Z., Peyman, D. A., & Ali, H. (2015) Assessment of Urban Heat Island based on the relationship between land surface temperature and Land Use/ Land Cover in Tehran. *Sustainable Cities and Society* 23 (2016) 94–104
27. Tyubee, B & Anyadike, R. (2012) Analysis of Surface Urban Heat Island in Makurdi, Nigeria. http://www.goes-r.gov/downloads/2012-AMS/poster01/296-Tyubee.pdf Last Accessed: 22/06/2017
28. Voogt, J.A., and Oke, T.R., (2003). Thermal remote sensing of urban climates. Remote Sensing of Environment, 86, 370-384.
29. Wang, Z., Wu, X., Yi, H., & Tongan, X. (2016) Studying the Urban Heat Island Using a Local Climate Zone Scheme. *Pol. J. Environ. Stud.* Vol. 25, No. 6 (2016), 2609-2616

30. Xin, H. (2016) Exploring the Influence of Urban Land Use and Land Cover Change on Land Surface Temperature Using Remote Sensing: A Case Study of Cuyahoga County, OH Master's Thesis Submitted to Department of Geography, Ohio University.
31. Yen-Ching, C., Hao-Wei, C., Yuan-Fong, S., Yii-Chen, W.,u, & Ke-Sheng, C.(2017) Does urbanization increase diurnal land surface temperature variation? Evidence and implications. *Landscape and Urban Planning* 157 (2017) 247–258
32. Yuan, F., & Bauer, M., (2007) Comparison of impervious surface area and normalized difference vegetation index as indicators of surface urban heat island effects in Landsat imagery . *Remote Sensing of Environment* 106 (2007) 375–386
33. Zhibin, R., Haifeng, Z., Xingyuan, H., Dan, Z., & Xingyang, Y.(2014) Estimation of the Relationship Between Urban Vegetation Configuration and Land Surface Temperature with Remote Sensing. *Indian Society of Remote Sensing 2014*. DOI 10.1007/s12524-014-0373-9
34. García-Díez, M., Lauwaet, D., Hooyberghs, H., Ballester, J., De Ridder, K., & Rodó, X.(2016) Advantages of using a fast urban boundary layer model as compared to a full mesoscale model to simulate the urban heat island of Barcelona, *Geosci. Model Dev*., 9, 4439-4450, https://doi.org/10.5194/gmd-9-4439-2016, 2016.
35. Gesch D.B, Oimoen. M.J and Evans G.A (2014) Accuracy Assessment of the US Geological Survey National Elevation Dataset and Comparison with Other large-area Data sets-SRTM and ASTER. US Geological Survey File Report 2014 -1008 10p
36. Jasim, M. A., Stuart, H. M., & Martin, J. S.(2016) Modelling the Spatiotemporal change of canopy urban heat islands. *Building and Environment 107 (2016)* 64-78
37. Jeppesen, H. (2013) Population Growth Challenges Poor Nations: Globalization. http://www.dw.com/en/population-growth-challenges-poor-nations/a-17010329 Accessed 05/10/2017
38. Jimoh, H.I. (2003), Erosion Tolerance Range of Landuse Surface: Implication on Land Resource Use and Management Techniques in Ilorin, Nigeria, Intern. Journal on *Environmental Studies*, 60(5) 445-452.
39. Kikon, N., Prafull, S., Sudhir, K. S., and Anjana, V. (2016) Assessment of Urban Heat Islands (UHI) of Noida City, India using multi-temporal satellite data: *Sustainable Cities & Society* , Vol. 22, p19-28,
40. Kwara State Ministry of Planning and Economic Development (2012).Attaining millennium development goals: Poverty eradication strategies. Presented at The NIPR annual general meeting and awards 2012. Ilorin: NIPR
41. Landsat 7 Users Data Hand Book (2001) https://landsat.gsfc.nasa.gov/wp-content/uploads/2016/08/Landsat7_Handbook.pdf#page=120&zoom=auto,-457,98
42. Landsat 8 Users Data Hand Book (2016) https://landsat.usgs.gov/sites/default/files/documents/Landsat8DataUsersHandbook.pdf. Last Accessed 29/09/2017
43. Marco, M., Alfonso, C., Alessandro, M., Simone, O., Antonio, R., Giampiero, M., Michele, M., (2016) The impact of built-up surfaces on land surface temperatures in Italian urban areas. *Science of the Total Environment* 551–552 (2016) 317–326
44. Nigeria Meteorological Agency (2013) https://nimet.gov.ng
45. Oke T.R., (1982) The Energetic Basis of the Urban Heat Island. *Quarterly Journal of the*

46. Olorunfemi, F. & Raheem, U. (2013). Urban Vulnerability and Adaptation to Extreme Weather Events: A Case Study of Rainstorm Victims in Ilorin, Nigeria. *Geography, Environment, Sustainability.* 2013;6(2):80-93 DOI 10.24057/2071-9388-2013-6-2-80-93
47. Quattrochi DA and Ridd MK (1994) Measurement and analysis of thermal energy responses from discrete urban surfaces using remote sensing data. International *Journal of Remote Sensing 15: 1991–2022*.
*Royal Meteorological Societ*y, 108, 1-24
48. Rybski and Kropp (2017) The Role of City Size and formation of Urban Heat Island. Scientific Reports. https://www.nature.com/articles/s41598-017-04242-2
49. Smith, C., Webb, A., Levermore, G.J., Lindley, S.J.,& Beswick, K. (2011) Fine-scale spatial temperature patterns across a UK conurbation. *Clim. Chang.* **2011**, *109*, 269–286
50. Streutker, D. R. (2002). A remote sensing study of the urban heat island of Houston, Texas. *International Journal of Remote Sensing*, 23, 2595 – 2608.
51. Streutker, D. R. (2003). Satellite-measured growth of the urban heat island of Houston, Texas. *Remote Sensing of Environment*, 85, 282 – 289.
52. U.S. Geological Survey (2015c) Landsat processing details. https://landsat.usgs.gov/Landsat-Processing-Details
53. UN-HABITAT (2006) United Nations Human Settlements Program. 2006 Annual Report. http://mirror.unhabitat.org/pmss/getElectronicVersion.aspx?nr=2343&alt=1 Last Accessed 17/07/2017
54. United Nations (2016) United Nations Urbanization and Development: Emerging Futures; World Cities Reports. http://wcr.unhabitat.org/wp-content/uploads/sites/16/2016/05/WCR-%20Full-Report-2016.pdf. Last accessed, 21/06/2017
55. Voogt, J.A & Oke, T.R (2003) Thermal remote sensing of urban climates. *Remote Sensing of Environment* **86**:3, 370-384.
56. Xinke, Z., Xing, H., Chao, R., Jelila, L., and Zhao-Liang, L. (2016) Retrieving Land Surface Temperature from Hyperspectral Thermal Infrared Data Using a Multi-Channel Method. *Sensors*, Vol 16 (5)
57. Yue, W. Z., & Xu, J. H. (2007). The relationship between land surface temperature and NDVI with remote sensing. *International Journal of Remote Sensing, 28*(15), 3205–3226
58. Zhao, L., Lee, X., Smith, R. B., and Oleson, K.(2014) Strong contributions of local background climate to urban heat islands, Nature, 511, 216–219, doi:10.1038/nature13462, 2014.

Appendix

Appendix 1: Estimation of NDVI from Landsat 7 and 8

Bands 3 and 4, and bands 4 and 5 are used for NDVI estimation for Landsats 7 and 8 respectively.

Step 2:

Appendix 2: NDVI Computation:

The equation for computing NDVI for both sensors is:

NDVI = (ρ nir - ρred)/ (ρnir + ρred) (Equation 8)

Where: *ρ nir* is the Near infrared band and

ρred is the Red band.

Appendix 3: Computation of Land Surface Emissivity (LSE)

e = 0.004Pv + 0.986, (Equation 9)

Where: ***e*** = emissivity, and

Pv = Proportional Vegetation.

However, ***Pv*** = $(NDVI - NDVI_{min}) / (NDVI_{max} - NDVI_{min})^2$ (Equation 9)

Series from Lund University

Department of Physical Geography and Ecosystem Science

Master Thesis in Geographical Information Science

1. *Anthony Lawther:* The application of GIS-based binary logistic regression for slope failure susceptibility mapping in the Western Grampian Mountains, Scotland (2008).
2. *Rickard Hansen:* Daily mobility in Grenoble Metropolitan Region, France. Applied GIS methods in time geographical research (2008).
3. *Emil Bayramov:* Environmental monitoring of bio-restoration activities using GIS and Remote Sensing (2009).
4. *Rafael Villarreal Pacheco:* Applications of Geographic Information Systems as an analytical and visualization tool for mass real estate valuation: a case study of Fontibon District, Bogota, Columbia (2009).
5. *Siri Oestreich Waage:* a case study of route solving for oversized transport: The use of GIS functionalities in transport of transformers, as part of maintaining a reliable power infrastructure (2010).
6. *Edgar Pimiento:* Shallow landslide susceptibility – Modelling and validation (2010).
7. *Martina Schäfer:* Near real-time mapping of floodwater mosquito breeding sites using aerial photographs (2010).
8. *August Pieter van Waarden-Nagel:* Land use evaluation to assess the outcome of the programme of rehabilitation measures for the river Rhine in the Netherlands (2010).
9. *Samira Muhammad:* Development and implementation of air quality data mart for Ontario, Canada: A case study of air quality in Ontario using OLAP tool. (2010).
10. *Fredros Oketch Okumu*: Using remotely sensed data to explore spatial and temporal relationships between photosynthetic productivity of vegetation and malaria transmission intensities in selected parts of Africa (2011).
11. *Svajunas Plunge:* Advanced decision support methods for solving diffuse water pollution problems (2011).
12. *Jonathan Higgins:* Monitoring urban growth in greater Lagos: A case study using GIS to monitor the urban growth of Lagos 1990 - 2008 and produce future growth prospects for the city (2011).
13. *Mårten Karlberg:* Mobile Map Client API: Design and Implementation for Android (2011).
14. *Jeanette McBride:* Mapping Chicago area urban tree canopy using color infrared imagery (2011).
15. *Andrew Farina:* Exploring the relationship between land surface temperature and vegetation abundance for urban heat island mitigation in Seville, Spain (2011).
16. *David Kanyari*: Nairobi City Journey Planner: An online and a Mobile Application (2011).

17. *Laura V. Drews:* Multi-criteria GIS analysis for siting of small wind power plants - A case study from Berlin (2012).
18. *Qaisar Nadeem:* Best living neighborhood in the city - A GIS based multi criteria evaluation of ArRiyadh City (2012).
19. *Ahmed Mohamed El Saeid Mustafa:* Development of a photo voltaic building rooftop integration analysis tool for GIS for Dokki District, Cairo, Egypt (2012).
20. *Daniel Patrick Taylor*: Eastern Oyster Aquaculture: Estuarine Remediation via Site Suitability and Spatially Explicit Carrying Capacity Modeling in Virginia's Chesapeake Bay (2013).
21. *Angeleta Oveta Wilson:* A Participatory GIS approach to *unearthing* Manchester's Cultural Heritage '*gold mine'* (2013).
22. *Ola Svensson:* Visibility and Tholos Tombs in the Messenian Landscape: A Comparative Case Study of the Pylian Hinterlands and the Soulima Valley (2013).
23. *Monika Ogden:* Land use impact on water quality in two river systems in South Africa (2013).
24. *Stefan Rova:* A GIS based approach assessing phosphorus load impact on Lake Flaten in Salem, Sweden (2013).
25. *Yann Buhot:* Analysis of the history of landscape changes over a period of 200 years. How can we predict past landscape pattern scenario and the impact on habitat diversity? (2013).
26. *Christina Fotiou:* Evaluating habitat suitability and spectral heterogeneity models to predict weed species presence (2014).
27. *Inese Linuza:* Accuracy Assessment in Glacier Change Analysis (2014).
28. *Agnieszka Griffin:* Domestic energy consumption and social living standards: a GIS analysis within the Greater London Authority area (2014).
29. *Brynja Guðmundsdóttir:* Detection of potential arable land with remote sensing and GIS - A Case Study for Kjósarhreppur (2014).
30. *Oleksandr Nekrasov:* Processing of MODIS Vegetation Indices for analysis of agricultural droughts in the southern Ukraine between the years 2000-2012 (2014).
31. *Sarah Tressel:* Recommendations for a polar Earth science portal in the context of Arctic Spatial Data Infrastructure (2014).
32. *Caroline Gevaert:* Combining Hyperspectral UAV and Multispectral Formosat-2 Imagery for Precision Agriculture Applications (2014).
33. *Salem Jamal-Uddeen:* Using GeoTools to implement the multi-criteria evaluation analysis - weighted linear combination model (2014).
34. *Samanah Seyedi-Shandiz:* Schematic representation of geographical railway network at the Swedish Transport Administration *(*2014).
35. *Kazi Masel Ullah:* Urban Land-use planning using Geographical Information System and analytical hierarchy process: case study Dhaka City (2014).
36. *Alexia Chang-Wailing Spitteler:* Development of a web application based on MCDA and GIS for the decision support of river and floodplain rehabilitation projects (2014).

37. *Alessandro De Martino:* Geographic accessibility analysis and evaluation of potential changes to the public transportation system in the City of Milan (2014).
38. *Alireza Mollasalehi:* GIS Based Modelling for Fuel Reduction Using Controlled Burn in Australia. Case Study: Logan City, QLD (2015).
39. *Negin A. Sanati:* Chronic Kidney Disease Mortality in Costa Rica; Geographical Distribution, Spatial Analysis and Non-traditional Risk Factors (2015).
40. *Karen McIntyre:* Benthic mapping of the Bluefields Bay fish sanctuary, Jamaica (2015).
41. *Kees van Duijvendijk:* Feasibility of a low-cost weather sensor network for agricultural purposes: A preliminary assessment (2015).
42. *Sebastian Andersson Hylander:* Evaluation of cultural ecosystem services using GIS (2015).
43. *Deborah Bowyer:* Measuring Urban Growth, Urban Form and Accessibility as Indicators of Urban Sprawl in Hamilton, New Zealand (2015).
44. *Stefan Arvidsson:* Relationship between tree species composition and phenology extracted from satellite data in Swedish forests (2015).
45. *Damián Giménez Cruz*: GIS-based optimal localisation of beekeeping in rural Kenya (2016).
46. *Alejandra Narváez Vallejo:* Can the introduction of the topographic indices in LPJ-GUESS improve the spatial representation of environmental variables? (2016).
47. *Anna Lundgren:* Development of a method for mapping the highest coastline in Sweden using breaklines extracted from high resolution digital elevation models (2016).
48. *Oluwatomi Esther Adejoro:* Does location also matter? A spatial analysis of social achievements of young South Australians (2016).
49. *Hristo Dobrev Tomov:* Automated temporal NDVI analysis over the Middle East for the period 1982 - 2010 (2016).
50. *Vincent Muller:* Impact of Security Context on Mobile Clinic Activities A GIS Multi Criteria Evaluation based on an MSF Humanitarian Mission in Cameroon (2016).
51. *Gezahagn Negash Seboka:* Spatial Assessment of NDVI as an Indicator of Desertification in Ethiopia using Remote Sensing and GIS (2016).
52. *Holly Buhler:* Evaluation of Interfacility Medical Transport Journey Times in Southeastern British Columbia. (2016).
53. *Lars Ole Grottenberg*: Assessing the ability to share spatial data between emergency management organisations in the High North (2016).
54. *Sean Grant:* The Right Tree in the Right Place: Using GIS to Maximize the Net Benefits from Urban Forests (2016).
55. *Irshad Jamal:* Multi-Criteria GIS Analysis for School Site Selection in Gorno-Badakhshan Autonomous Oblast, Tajikistan (2016).
56. *Fulgencio Sanmartín:* Wisdom-volkano: A novel tool based on open GIS and time-series visualization to analyse and share volcanic data (2016).

57. *Nezha Acil:* Remote sensing-based monitoring of snow cover dynamics and its influence on vegetation growth in the Middle Atlas Mountains (2016).
58. *Julia Hjalmarsson:* A Weighty Issue: Estimation of Fire Size with Geographically Weighted Logistic Regression (2016).
59. *Mathewos Tamiru Amato:* Using multi-criteria evaluation and GIS for chronic food and nutrition insecurity indicators analysis in Ethiopia (2016).
60. *Karim Alaa El Din Mohamed Soliman El Attar:* Bicycling Suitability in Downtown, Cairo, Egypt (2016).
61. *Gilbert Akol Echelai:* Asset Management: Integrating GIS as a Decision Support Tool in Meter Management in National Water and Sewerage Corporation (2016).
62. *Terje Slinning:* Analytic comparison of multibeam echo soundings (2016).
63. *Gréta Hlín Sveinsdóttir:* GIS-based MCDA for decision support: A framework for wind farm siting in Iceland (2017).
64. *Jonas Sjögren:* Consequences of a flood in Kristianstad, Sweden: A GIS-based analysis of impacts on important societal functions (2017).
65. *Nadine Raska:* 3D geologic subsurface modelling within the Mackenzie Plain, Northwest Territories, Canada (2017).
66. *Panagiotis Symeonidis*: Study of spatial and temporal variation of atmospheric optical parameters and their relation with PM 2.5 concentration over Europe using GIS technologies (2017).
67. *Michaela Bobeck:* A GIS-based Multi-Criteria Decision Analysis of Wind Farm Site Suitability in New South Wales, Australia, from a Sustainable Development Perspective (2017).
68. *Raghdaa Eissa*: Developing a GIS Model for the Assessment of Outdoor Recreational Facilities in New Cities Case Study: Tenth of Ramadan City, Egypt (2017).
69. *Zahra Khais Shahid*: Biofuel plantations and isoprene emissions in Svea and Götaland (2017).
70. *Mirza Amir Liaquat Baig*: Using geographical information systems in epidemiology: Mapping and analyzing occurrence of diarrhea in urban - residential area of Islamabad, Pakistan (2017).
71. *Joakim Jörwall*: Quantitative model of Present and Future well-being in the EU-28: A spatial Multi-Criteria Evaluation of socioeconomic and climatic comfort factors (2017).
72. *Elin Haettner*: Energy Poverty in the Dublin Region: Modelling Geographies of Risk (2017).
73. *Harry Eriksson*: Geochemistry of stream plants and its statistical relations to soil- and bedrock geology, slope directions and till geochemistry. A GIS-analysis of small catchments in northern Sweden (2017).
74. *Daniel Gardevärn:* PPGIS and Public meetings – An evaluation of public participation methods for urban planning (2017).
75. *Kim Friberg:* Sensitivity Analysis and Calibration of Multi Energy Balance Land Surface Model Parameters (2017).
76. *Viktor Svanerud:* Taking the bus to the park? A study of accessibility to green areas in Gothenburg through different modes of transport (2017).

77. *Lisa-Gaye Greene*: Deadly Designs: The Impact of Road Design on Road Crash Patterns along Jamaica's North Coast Highway (2017).
78. *Katarina Jemec Parker*: Spatial and temporal analysis of fecal indicator bacteria concentrations in beach water in San Diego, California (2017).
79. *Angela Kabiru*: An Exploratory Study of Middle Stone Age and Later Stone Age Site Locations in Kenya's Central Rift Valley Using Landscape Analysis: A GIS Approach (2017).
80. *Kristean Björkmann*: Subjective Well-Being and Environment: A GIS-Based Analysis (2018).
81. *Williams Erhunmonmen Ojo*: Measuring spatial accessibility to healthcare for people living with HIV-AIDS in southern Nigeria (2018).
82. *Daniel Assefa*: Developing Data Extraction and Dynamic Data Visualization (Styling) Modules for Web GIS Risk Assessment System (WGRAS). (2018).
83. *Adela Nistora*: Inundation scenarios in a changing climate: assessing potential impacts of sea-level rise on the coast of South-East England (2018).
84. *Marc Seliger*: Thirsty landscapes - Investigating growing irrigation water consumption and potential conservation measures within Utah's largest master-planned community: Daybreak (2018).
85. *Luka Jovičić*: Spatial Data Harmonisation in Regional Context in Accordance with INSPIRE Implementing Rules (2018).
86. *Christina Kourdounouli*: Analysis of Urban Ecosystem Condition Indicators for the Large Urban Zones and City Cores in EU (2018).
87. *Jeremy Azzopardi*: Effect of distance measures and feature representations on distance-based accessibility measures (2018).
88. *Patrick Kabatha*: An open source web GIS tool for analysis and visualization of elephant GPS telemetry data, alongside environmental and anthropogenic variables (2018).
89. *Richard Alphonce Giliba*: Effects of Climate Change on Potential Geographical Distribution of Prunus africana (African cherry) in the Eastern Arc Mountain Forests of Tanzania (2018).
90. *Eiður Kristinn Eiðsson*: Transformation and linking of authoritative multi-scale geodata for the Semantic Web: A case study of Swedish national building data sets (2018).
91. *Niamh Harty*: HOP!: a PGIS and citizen science approach to monitoring the condition of upland paths (2018).
92. *José Estuardo Jara Alvear*: Solar photovoltaic potential to complement hydropower in Ecuador: A GIS-based framework of analysis (2018).
93. *Brendan O'Neill*: Multicriteria Site Suitability for Algal Biofuel Production Facilities (2018).
94. *Roman Spataru*: Spatial-temporal GIS analysis in public health – a case study of polio disease (2018).
95. *Alicja Miodońska*: Assessing evolution of ice caps in Suðurland, Iceland, in years 1986 - 2014, using multispectral satellite imagery (2019).
96. *Dennis Lindell Schettini*: A Spatial Analysis of Homicide Crime's Distribution and Association with Deprivation in Stockholm Between 2010-2017 (2019).

97. *Damiano Vesentini*: The Po Delta Biosphere Reserve: Management challenges and priorities deriving from anthropogenic pressure and sea level rise (2019).
98. *Emilie Arnesten*: Impacts of future sea level rise and high water on roads, railways and environmental objects: a GIS analysis of the potential effects of increasing sea levels and highest projected high water in Scania, Sweden (2019).
99. *Syed Muhammad Amir Raza*: Comparison of geospatial support in RDF stores: Evaluation for ICOS Carbon Portal metadata (2019).
100. *Hemin Tofiq*: Investigating the accuracy of Digital Elevation Models from UAV images in areas with low contrast: A sandy beach as a case study (2019).
101. *Evangelos Vafeiadis*: Exploring the distribution of accessibility by public transport using spatial analysis. A case study for retail concentrations and public hospitals in Athens (2019).
102. *Milan Sekulic*: Multi-Criteria GIS modelling for optimal alignment of roadway by-passes in the Tlokweng Planning Area, Botswana (2019).
103. *Ingrid Piirisaar*: A multi-criteria GIS analysis for siting of utility-scale photovoltaic solar plants in county Kilkenny, Ireland (2019).
104. *Nigel Fox*: Plant phenology and climate change: possible effect on the onset of various wild plant species' first flowering day in the UK (2019).
105. *Gunnar Hesch*: Linking conflict events and cropland development in Afghanistan, 2001 to 2011, using MODIS land cover data and Uppsala Conflict Data Programme (2019).
106. *Elijah Njoku*: Analysis of spatial-temporal pattern of Land Surface Temperature (LST) due to NDVI and elevation in Ilorin, Nigeria (2019).